

# MULTI-POINT AERODYNAMIC SHAPE DESIGN

by

Samy Elias

A thesis submitted in conformity with the requirements  
for the degree of Masters of Applied Science  
Graduate Department of Aerospace Engineering  
University of Toronto

Copyright © 2005 by Samy Elias



# Abstract

## Multi-Point Aerodynamic Shape Design

Samy Elias

Masters of Applied Science

Graduate Department of Aerospace Engineering

University of Toronto

2005

This thesis examines several aspects of multi-point aerodynamic shape optimization in two dimensions, including testing of an automated weighting formula, automated introduction of design points, and three methods of imposing geometric constraints. A quasi-Newton algorithm is used, with a quadratic penalty approach for the constraints. A Newton-Krylov algorithm is used to solve the compressible Navier-Stokes equations; the same Krylov algorithm is used to solve the discrete adjoint problem to calculate the gradient. Several different multi-point problems with varying Mach number and target lift coefficients are examined to consider trade-offs in the solution and design point weighting. The automated weighting formula and automated design point addition successfully achieve optimization over a broad range of Mach numbers. The floating thickness and area constraints prove advantageous in providing more flexibility in the optimization.



## Acknowledgements

I would like to thank my friends and family for their support. I would also like to thank Prof. D. W. Zingg for his guidance and professionalism, and Marian Nemeč for his help.



# Contents

<b>Abstract</b>	<b>iv</b>
<b>Acknowledgments</b>	<b>v</b>
<b>Contents</b>	<b>viii</b>
<b>List of Tables</b>	<b>ix</b>
<b>List of Figures</b>	<b>xii</b>
<b>List of Symbols</b>	<b>xiii</b>
<b>1 Introduction</b>	<b>1</b>
1.1 Motivation . . . . .	1
1.2 OPTIMA Background . . . . .	2
1.3 Objectives . . . . .	3
<b>2 Pareto Fronts</b>	<b>5</b>
2.1 Fixed Mach Number, Varied Lift Coefficient Targets . . . . .	5
2.2 Fixed Lift Coefficient Target, Varied Mach Numbers . . . . .	7
<b>3 Generalized Shape Constraints</b>	<b>11</b>
3.1 Area and Floating Thickness Constraints . . . . .	11
3.2 Results . . . . .	12
<b>4 Automatic Weighting Technique</b>	<b>21</b>
4.1 Method . . . . .	21
4.2 Results . . . . .	22
<b>5 Multiple Mach Number and Lift Coefficient Problems</b>	<b>41</b>
5.1 Nine-point General Cases . . . . .	41
5.2 Nine-point Automated Weights Cases . . . . .	49

<b>6 Conclusions</b>	<b>57</b>
<b>References</b>	<b>60</b>

# List of Tables

2.1	$C_D$ at the design points for various values of $w$ . . . . .	8
4.1	Weights for Case 1: 13 DV, $c = 30$ . . . . .	24
4.2	Results for Case 1: 13 DV, $c = 30$ . . . . .	24
4.3	Weights for Case 2: 13 DV, $c = 15$ , Standard Deviation method . . . . .	27
4.4	Results for Case 2: 13 DV, $c = 15$ , Standard Deviation method . . . . .	27
4.5	Weights for Case 3: 13 DV, $c = 30$ , Half Standard Deviation method . . . . .	28
4.6	Results for Case 3: 13 DV, $c = 30$ , Half Standard Deviation method . . . . .	28
4.7	Weights for Case 4: 13 DV, $c = 15$ . . . . .	30
4.8	Results for Case 4: 13 DV, $c = 15$ . . . . .	30
4.9	Weights for Case 5: 13 DV, $c = 15$ , Half Standard Deviation method . . . . .	32
4.10	Results for Case 5: 13 DV, $c = 15$ , Half Standard Deviation method . . . . .	32
4.11	Weights for Case 6: 23 DV, $c = 30$ . . . . .	36
4.12	Results for Case 6: 23 DV, $c = 30$ . . . . .	36
4.13	Weights for Case 7: 23 DV, $c = 15$ . . . . .	37
4.14	Results for Case 7: 23 DV, $c = 15$ . . . . .	37
5.1	Nine-point Case 5 weights. . . . .	50
5.2	Nine-point Case 5 drag coefficients. . . . .	50
5.3	Nine-point Case 5 performance characteristics. . . . .	50
5.4	Nine-point Case 6 weights. . . . .	53
5.5	Nine-point Case 6 drag coefficients. . . . .	53
5.6	Nine-point Case 6 performance characteristics. . . . .	53



# List of Figures

2.1	Pareto front from both objective functions and drag coefficient. Weights: $\omega_L=1.0$ , $\omega_D=0.5$ , $\omega_P=1.0$ . . . . .	6
2.2	Assorted airfoils on the Pareto front. . . . .	7
2.3	Drag coefficient Pareto front for fixed $C_D$ varied $M$ case, with zoomed out view. . . . .	8
2.4	Mach number/drag sweeps for various weights. . . . .	9
2.5	Mach number/drag sweeps and airfoils for various best cases. . . . .	10
3.1	Single-point constraint cases. . . . .	13
3.2	Pressure distribution for the single-point alternative constraint cases. . . . .	14
3.3	Single-point fixed thickness cases, $C_P$ distribution. . . . .	15
3.4	Mach number contour graphs for the single-point area and floating thickness constraint cases. . . . .	15
3.5	Initial airfoil RAE2822 at $M = 76$ , $C_L=733$ . . . . .	16
3.6	Mach number contour graphs for the single-point fixed thickness cases. . . . .	16
3.7	Mach number/drag sweeps and airfoils for the 4-point constraint cases. . . . .	17
3.8	$C_P$ distribution for the 4-point constraint cases at $M=0.76$ . . . . .	18
3.9	Mach number contour graph for the 4-point area and floating thickness constraint cases, at $M=0.76$ and $C_L=0.733$ . . . . .	19
3.10	Mach number contour graph for the 4-point fixed thickness case, at $M=0.76$ and $C_L=0.733$ . . . . .	19
4.1	Case 1, 13 design variables, $c = 30$ ; Mach number/drag sweeps and airfoil . . . .	23
4.2	Case 1, $C_p$ graphs for all five design points, for $C_l = 0.733$ . . . . .	25
4.3	Case 1, 13 DV, $c = 30$ ; Mach number contour graph at $M=0.76$ , $C_L=0.733$ . . . .	26
4.4	Case 2, 13 DV, $c = 30$ , standard deviation method; Mach number/drag sweeps .	27
4.5	Case 3, 13 DV, $c = 30$ , half standard deviation method; Mach number/drag sweeps	28
4.6	Standard deviation of drag and maximum drag at the design points ( $C_L = 0.733$ ) for cases 1-3. . . . .	29
4.7	Case 4, 13 DV, $c = 15$ ; Mach number/drag sweeps . . . . .	29
4.8	Case 5, 13 DV, $c = 15$ , half standard deviation method; Mach number/drag sweeps	31

4.9	Standard deviation of drag and maximum drag at the design points ( $C_L = 0.733$ ) for cases 4 and 5. . . . .	33
4.10	Standard deviation of drag and maximum drag at the design points ( $C_L = 0.733$ ) for cases 1 and 4. . . . .	33
4.11	Final Mach number/drag sweeps for all automated weight cases. . . . .	34
4.12	Case 6, 23 DV, $c = 30$ ; Mach number/drag sweeps . . . . .	34
4.13	Standard deviation of drag and maximum drag at the design points ( $C_L = 0.733$ ) for cases 1, 6 and 7. . . . .	35
4.14	Case 7, 23 DV, $c = 15$ ; Mach number/drag sweeps and airfoil . . . . .	38
4.15	Case 7, 23 DV, $c = 15$ ; Mach number contour graph at $M=0.76$ , $C_L=0.733$ . . . . .	38
4.16	Case 7, $C_p$ graphs for all five design points, for $C_l = 0.733$ . . . . .	39
5.1	Nine-point Case 1. . . . .	42
5.2	RAE 2822 Mach number contour graph at a) $M=0.76$ , $C_L=0.733$ , b) $M=0.76$ , $C_L=0.77$ . . . . .	43
5.3	Nine-point Case 1 Mach number contour graph at a) $M=0.76$ , $C_L=0.733$ , b) $M=0.76$ , $C_L=0.77$ . . . . .	43
5.4	Nine-point Case 2 (23 DV instead of 13 DV). . . . .	44
5.5	Nine-point Case 2 Mach number contour graph at a) $M=0.76$ , $C_L=0.733$ , b) $M=0.76$ , $C_L=0.77$ . . . . .	45
5.6	Comparison of Mach number/drag sweeps for the nine-point Cases 1 and 2 (13 DV vs. 23 DV). . . . .	45
5.7	Nine-point Case 3. . . . .	46
5.8	Mach number contour graph at $M=0.76$ , $C_L=0.75$ , for a) RAE 2822, b) Case 3. . . . .	47
5.9	Nine-point Case 4. . . . .	47
5.10	Mach number contour graph at $M=0.73$ , $C_L=0.74$ , for a) RAE 2822, b) Case 4. . . . .	48
5.11	Final airfoils for nine-point cases 3 and 4. . . . .	48
5.12	Mach number/drag sweeps and airfoils for nine-point Cases 5 and 6. . . . .	51
5.13	Nine-point Case 6 Mach number contour graph at a) $M=0.76$ , $C_L=0.733$ , b) $M=0.76$ , $C_L=0.77$ . . . . .	52
5.14	Case 6, $C_p$ graphs for all nine design points. . . . .	54
5.15	Comparison of Mach number/drag sweeps for the nine-point Cases 1, 2, and 6. . . . .	55
5.16	Comparison of airfoils for nine-point Cases 1, 2, and 6. . . . .	56

# List of Symbols

$\alpha$	angle of attack
$A$	airfoil area
$A^*$	target airfoil area
$c$	chord length of airfoil
$c$	user defined constant for automated weighting cases
$C_D$	coefficient of drag
$C_L$	coefficient of lift
$C_D^*$	target coefficient of drag
$C_L^*$	target coefficient of lift
$\mathcal{J}$	objective function
$M$	Mach number
$M_\infty$	freestream Mach number
$Q$	vector of conservative variables
$P$	objective function penalty term
$P_{area}$	objective function penalty term for an area constraint
$t$	airfoil thickness
$w$	design point weighting for multi-point optimization
$\omega_D$	weighting of drag objective function term
$\omega_L$	weighting of lift objective function term
$\omega_P$	weighting of penalty term
$x, y$	coordinates in the physical domain
$X$	vector of design variables



# Chapter 1

## Introduction

### 1.1 Motivation

In order to improve the performance of an airfoil under certain flow conditions, a combination of analysis and shape modification is used to determine the best solution to a particular problem. Numerical optimization is one of the methods used in this process. It allows a designer to specify one or more sets of operating conditions and the aerodynamic properties desired at those design points, such as increasing lift or reducing drag. Since the process of modifying the shape is governed automatically by the numerical optimization process chosen, the focus of the designer is in properly formulating the problem, with the strengths and weaknesses of the optimizer in mind, as well as the general restrictions of physical flow. The design objectives and design points need to be chosen so as not to neglect a mode of operation that can be severely disadvantaged if ignored.

Gradient-based methods and genetic algorithms are two of the favoured numerical optimization methods. Genetic algorithms, based on the idea of natural selection and mating of designs to produce an optimal design [10, 6, 16, 25, 27, 34, 32], is, as the nature of the process would suggest, slow, and requires considerable computation to generate and analyze a viable mating population [22, 30, 11]. Gradient-based optimization offers a more focussed and less computationally intensive method [9, 4, 24, 14, 18]. A local optimum can be found with gradient-based methods using far fewer computational iterations. This advantage is partly due to effective gradient calculation and convergence methods, such as adjoint methods and the Newton-Krylov algorithm, by Nemec and Zingg [21]. The Newton-Krylov method, among the fastest of numerical algorithms, is not only a fast flow solver, but the preconditioned generalized minimum residual (GMRES) method [28] used in its application can also be used to solve for the objec-

tive function gradient, therefore saving on computational costs. Using quasi-Newton methods, the gradient-based optimization method can be used to calculate the search direction in an optimization, and approximate the curvature in the design space from the current solution.

Although the quasi-Newton strategy can be used in the context of an unconstrained optimization problem, this requires careful attention in choosing the design variables and formulating the objective function [3, 13, 29]. Volume and thickness requirements tend to be necessary [7]. The design objectives need to be balanced against these constraints, and need to be implemented in a way that offers the optimizing process the required flexibility to reach a best solution. Typically these constraints are formed as a penalty function [17], but one alternative is to use an SQP algorithm like SNOPT [8]. The Kreisselmeier-Steinhauser (KS) function [33, 1, 23, 2] is another common method.

There are many comparisons of gradient-based strategies being used for aerodynamic optimization. Obayashi [26] compared such a strategy to genetic algorithms for a transonic wing design, while Weinerfelt [31] did the same for an ONERA M6 wing, with a lift-constrained drag minimization problem. Leoviriyakit and Jameson [14] use the continuous adjoint method to converge the flow solution, sensitivities, and final shape. The importance of using several design points becomes clear when solutions show undesirable performance at the off-design points [18], and examining Pareto fronts to evaluate the variety of optimum solutions and their trade-offs becomes part of the design process [32]. Typically a weighted-sum approach is used towards the objective function in multi-point design, for example in another ONERA M6 wing optimization [34]. Since the weighting on each design point can play a role in the optimization solution, the designer's careful input is required in choosing these weights, or in choosing a method for altering the weightings as a function of the performance, such as by Li, Huyse, and Padula [15]. Another method of avoiding point-optimization effects is to minimize the derivative of the drag coefficient with respect to  $M_\infty$  [12].

## 1.2 OPTIMA Background

One of the optimization packages developed by the CFD group at UTIAS is OPTIMA2D, an airfoil shape optimizer for single-block grids about single-element airfoils [19]. A Newton-Krylov algorithm is used with the discrete-adjoint method to calculate the gradient of the objective function. The adjoint equation

$$\frac{\partial F^T}{\partial Q} \psi = \frac{\partial J^T}{\partial Q} \quad (1.1)$$

is solved using the preconditioned generalized minimal residual (GMRES) method [28]; the adjoint variables,  $\psi$ , are then used to solve the for gradient:

$$\frac{dJ}{dX} = \frac{\partial J}{\partial X} - \psi^T \frac{\partial F}{\partial X} \quad (1.2)$$

where  $\mathcal{J}$  is the objective function,  $F(Q, X)$  is the flow equation,  $Q$  is the vector of flow variables, and  $X$  is the vector of design variables. GMRES is also used in conjunction with an inexact-Newton approach to obtain flow solutions [22]. Typical optimization problems include lift and drag optimization, multi-point problems, lift-to-drag ratio, and others [20]. Constraints are applied using a penalty formulation, forming an unconstrained problem, which is solved using a quasi-Newton method. One possible objective function can be expressed as:

$$\mathcal{J}|_{M_i} = \omega_D \left(1 - \frac{C_D}{C_D^*}\right)^2 + \omega_L \left(1 - \frac{C_L}{C_L^*}\right)^2 + \omega_P P \quad (1.3)$$

$C_l^*$  and  $C_d^*$  are the targets for a lift and drag optimization problem,  $P$  is the penalty function (typically thickness constraints), and  $\omega_D$ ,  $\omega_L$ , and  $\omega_P$  are weights.

For several Mach number values, to avoid the poor performance of point-optimized problems [5], the weighted sum can be written as

$$\mathcal{J}_M = \sum_{i=1}^n w_i \mathcal{J}_{M_i} \quad (1.4)$$

Each Mach number has its own angle of attack  $\alpha$  as a design variable.

### 1.3 Objectives

Using OPTIMA2D to solve multi-point aerodynamic shape optimization problems, the purpose of this thesis is to:

1. Examine the trade-offs in performance between design points in several different multi-point problems, as well as the relative importance of certain design points in the optimization process.
2. Test the use of more generalized geometric constraints as alternatives to a fixed-chord-location thickness constraint.

3. Evaluate the use of an automated weighting method for the design point weights and the automated introduction of additional design points to achieve a desired performance over a range of operating conditions.

## Chapter 2

# Pareto Fronts

### 2.1 Fixed Mach Number, Varied Lift Coefficient Targets

Two simple two-point cases are studied to illustrate the ideas of design trade-offs and multi-point optimization. It also allows us to examine the results as a Pareto front. In the first example, the two design points have flow conditions at the same Mach number, but the lift coefficient targets,  $C_L^*$ , are different. Both design points use the same objective function formulation:

$$\mathcal{J}_i = \begin{cases} \omega_D \left(1 - \frac{C_D}{C_D^*}\right)^2 + \omega_L \left(1 - \frac{C_L}{C_L^*}\right)^2 & \text{if } C_D > C_D^* \\ \omega_D \left(1 - \frac{C_D}{C_D^*}\right)^2 & \text{otherwise} \end{cases} \quad (2.1)$$

$C_L^*$  and  $C_D^*$  are the lift and drag coefficient targets. Since the desired optimization problem is lift-constrained drag minimization, an attainable lift coefficient target is chosen along with an unattainable drag coefficient target.  $\omega_L$  and  $\omega_D$  are the weightings for the two components; thickness constraints are added as a penalty term.

Fully turbulent flow is assumed, at a freestream Mach number of 0.75 and a Reynolds number of nine million. The lift coefficient targets for the two different optimization points are 0.65 and 0.715, with a drag coefficient target of 0.01. The initial design shape is the RAE 2822 airfoil, parametrized by a 15-point fourth-degree B-spline curve. All the spline control points are free except three at the leading edge, and the trailing edge point. Since the trailing edge is defined by two coincident points, this means there are 10 geometric design variables, with the angle of attack added as an eleventh design variable. In order to preserve a minimum thickness and prevent the surfaces from crossing, the following thickness constraints are used:  $t/c \geq 0.121$  at

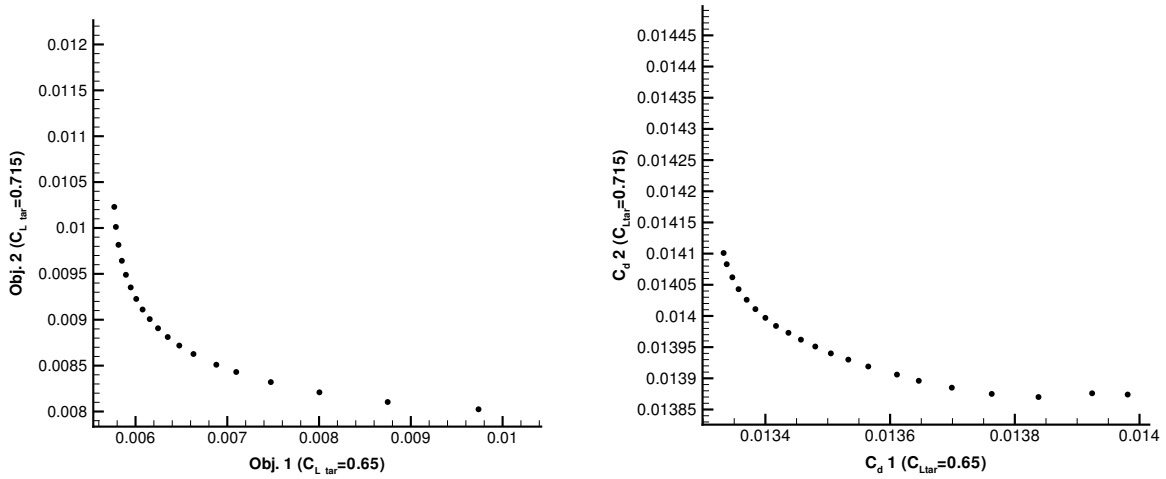


Figure 2.1: Pareto front from both objective functions and drag coefficient. Weights:  $\omega_L=1.0$ ,  $\omega_D=0.5$ ,  $\omega_P=1.0$

$x/c = 0.25$ ,  $t/c \geq 0.009$  at  $x/c = 0.92$ , and  $t/c \geq 0.002$  at  $x/c = 0.99$ . The weights in Eq. 1.3 are set to  $\omega_L=1.0$  and  $\omega_D=0.05$ , to force drag optimization near the intended  $C_L$  target. The thickness constraint penalty weight is  $\omega_P=1.0$ .

In order to frame the problem to produce a Pareto front, the following composite objective function is used:

$$\mathcal{J} = w\mathcal{J}_{C_L=0.65} + (1 - w)\mathcal{J}_{C_L=0.715} \quad (2.2)$$

where  $\mathcal{J}_{C_L=0.65}$  is the objective function evaluated using  $C_L^* = 0.65$  in Eq. 1.3, with  $\mathcal{J}_{C_L=0.715}$  treated likewise.  $w$  is the weight on the  $C_L=0.715$  condition. By using a range of values for  $w$  between 0.05 and 0.95 in increments of 0.05 (and including  $w=0.01$  as the topmost point), the Pareto fronts in Figure 2.1 are generated. The first shows the second objective function,  $\mathcal{J}_{C_L=0.715}$ , plotted against the first  $\mathcal{J}_{C_L=0.65}$ , whereas the second shows the drag coefficient at the target lift coefficients plotted against each other. The resulting Pareto front for the objective functions is smooth as expected, showing an apparently smooth trade-off curve between the two design points. The same is apparent in the second figure, save the last two points, which is easily explained by the other terms in the objective function defined in Eq. 1.3. The trade-off, though, while smooth, is not even. Reducing  $\mathcal{J}_{C_L=0.715}$  by 0.002 costs an increase of roughly 0.004 in  $\mathcal{J}_{C_L=0.65}$ . This means that focussing on the higher  $C_L$  target by giving it a higher weight in Eq. 2.2 will result in a larger sacrifice on the lower  $C_L^*$  final design than vice versa. Three different final airfoil shapes are shown in Figure 2.2.

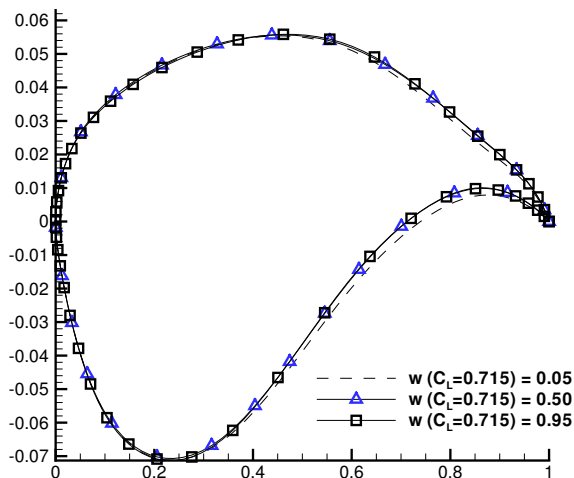


Figure 2.2: Assorted airfoils on the Pareto front.

## 2.2 Fixed Lift Coefficient Target, Varied Mach Numbers

In the second two-point case, the  $C_L$  target is the same for both points, but the Mach number is different. The two Mach numbers used are  $M=0.75$  and  $M=0.68$ , with a common  $C_L$  target of 0.715.  $\omega_L=1.0$  and  $\omega_D=0.1$  are used. All other conditions are the same as in the previous Pareto front case.  $w$  is the weight on the design point at  $M=0.75$ .

Figure 2.3 shows the drag coefficient Pareto front from plotting the drag coefficient at  $M=0.75$  and  $C_L=0.715$  vs. the drag coefficient at  $M=0.68$  and  $C_L=0.715$ , for varying  $w$ . In these figures the two axes use equal spacing, showing the unequal trade-off between the two design points. The drag coefficients at the design points are also listed in Table 2.1. There is a sharp drop in drag coefficient at  $M=0.75$  between  $w=0.1$  and  $w=0.55$ , showing very little drag coefficient gain at  $M=0.68$  for a considerable reduction of  $C_D$  at  $M=0.75$ . Although theoretically all points on a Pareto front are considered optimums, the severe trade-off in this case makes the optimum solution at  $w=0.55$  at a glance far more desirable than any lower values, from a designer's point of view.

Further exploring these results, the drag coefficient at  $C_L=0.715$  is plotted vs.  $M$  in Figure 2.4 for the various  $w$  values. Very small reductions in  $C_D$  at  $M=0.75$  are offset by far worse performance over the rest of the Mach number range shown. Between  $w=0.8$  and 0.9, for example, only a small reduction of 0.2% from  $C_D=0.014067$  to  $C_D=0.014043$  at  $M=0.75$  is gained for a much worse general performance between  $M=0.72$  and  $M=0.65$ ; at  $M=0.68$ ,  $C_D$

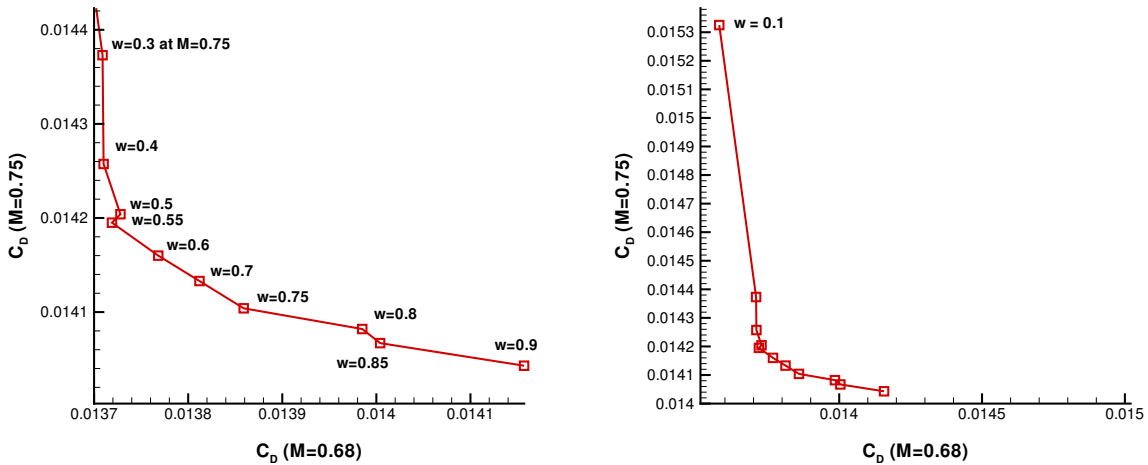


Figure 2.3: Drag coefficient Pareto front for fixed  $C_D$  varied  $M$  case, with zoomed out view.

Table 2.1:  $C_D$  at the design points for various values of  $w$ .

$w$	$C_D$ at	
	$M=0.75$	$M=0.68$
0.1	0.015325	0.013580
0.3	0.014373	0.013709
0.5	0.014204	0.013728
0.55	0.014195	0.013719
0.7	0.014133	0.013812
0.75	0.014104	0.013859
0.8	0.014082	0.013985
0.85	0.014067	0.014004
0.9	0.014043	0.014157

is increased by 1% from 0.014004 to 0.014157, a comparably large trade-off.

Selection of the most appropriate design depends on the designer's priorities. Some possible quantitative goals are: 1) minimizing the area under the  $C_D$  vs.  $M$  curve between the design points, 2) minimizing the maximum  $C_D$  for the design points, 3) minimizing the maximum  $C_D$  between and at the design points, or 4) equal drag for the design points. The minimum area is achieved with  $w=0.1$ ; this is also the worst design for reducing the drag coefficient at  $M=0.75$ . The best design for the second condition, minimizing the maximum  $C_D$  at the design points, is at  $w=0.85$ . This design also has the most equal drag coefficients between the design points. However, if we consider maximum  $C_D$  between the design points as well, minimizing this gives  $w=0.55$  as the best value. Note that the performance at lower Mach numbers is greatly improved from  $w=0.85$ , for a small increase in  $C_D$  at  $M=0.75$ , as shown in Figure 2.5, which also shows the final airfoil shapes. These examples illustrate the various trade-offs involved in determining which design is the most desirable.

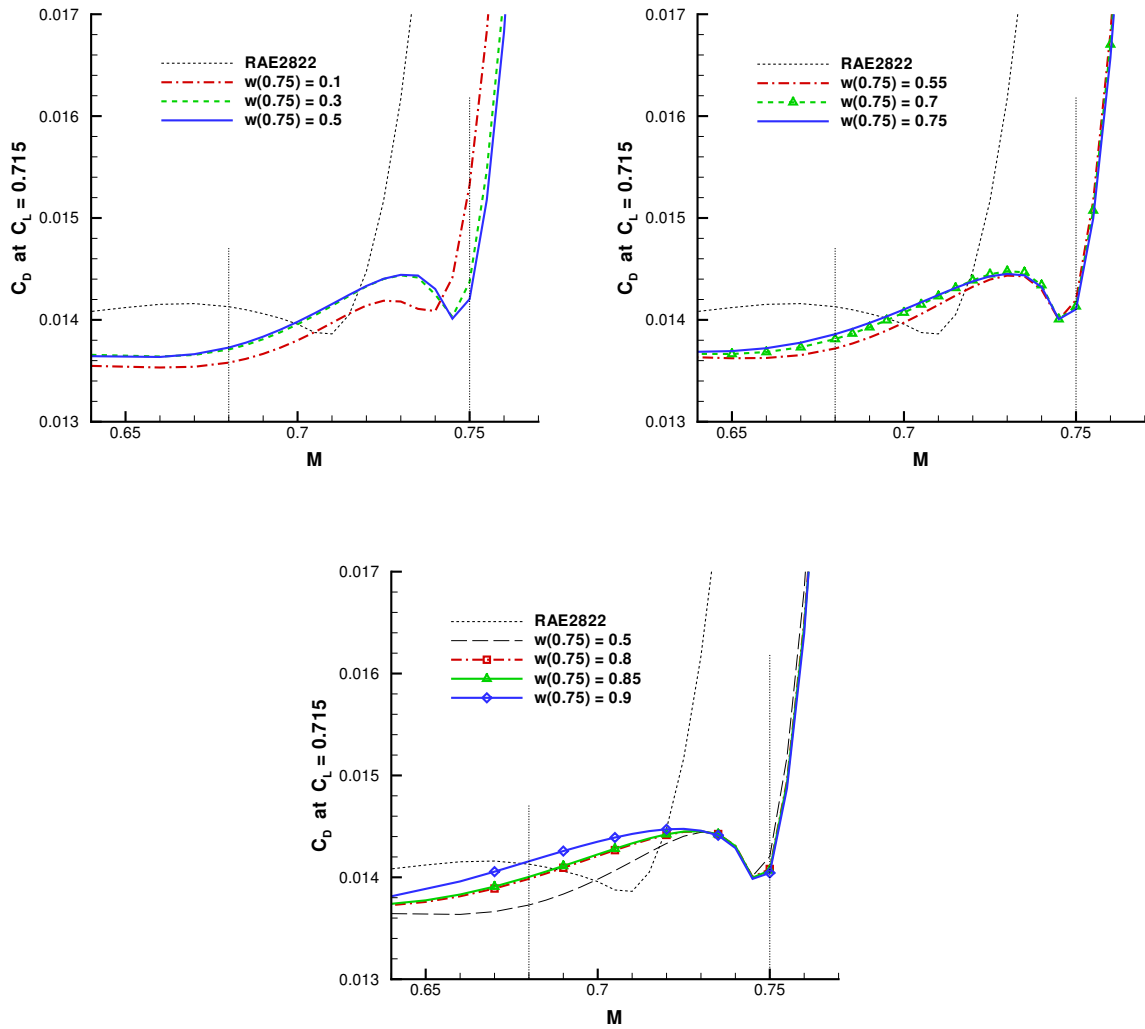


Figure 2.4: Mach number/drag sweeps for various weights.

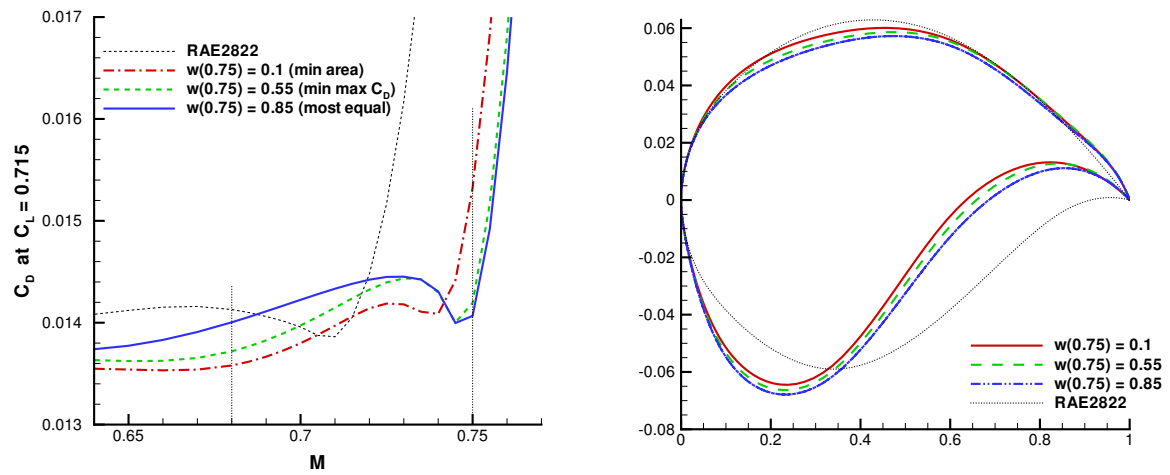


Figure 2.5: Mach number/drag sweeps and airfoils for various best cases.

## Chapter 3

# Generalized Shape Constraints

### 3.1 Area and Floating Thickness Constraints

One of the primary constraints in these optimization problems, and in general, are minimum thickness requirements on the designed airfoil. These are usually mandated by structural strength requirements and the need to store fuel in the wing. The usual method in the cases in this thesis is to define a minimum thickness at a certain percentage of the chord. However, this might unnecessarily constrain the problem, since the choice of the chord location is fixed and needs to be chosen by the designer. Allowing more flexible constraint terms can allow the optimization to find a better solution which may have been excluded by a poorly chosen minimum thickness size and location.

One alternative is to use the area of the two-dimensional airfoil as a constraint. This could be analogous to choosing a minimum volume for a wing fuel tank. The penalty term is defined as:

$$P_{area} = \omega_P \frac{A}{A^*} \quad (3.1)$$

where  $A$  and  $A^*$  are the current and target area, respectively, and  $\omega_P$  is the weighting on the penalty term.

Another method is to define a minimum thickness as before, but without setting a fixed location where this condition has to be met. Instead, a range of  $x$  on the chord is defined where this minimum thickness can be met. In other words, the new constraint, a floating thickness constraint, allows the minimum thickness constraint to be satisfied anywhere in a certain  $x$  range on the chord instead of one location. Other than checking over a range to determine the

$x$  location, the penalty formulation is the same as for a fixed thickness constraint.

## 3.2 Results

These alternative constraint methods are tested on both single and four-point optimization problems. Starting with the single-point cases,  $C_L^*=0.733$  and  $C_D^*=0.012$  are used, with weights  $\omega_L=1.0$ ,  $\omega_D=0.1$ , and  $\omega_P=1.0$ . The flow is assumed to be fully turbulent, with freestream Mach number  $M=0.76$  at a Reynolds number of 2.7 million. For the initial geometry the RAE 2822 is used, parametrized again with a 15 control point B-spline curve. Only the leading edge and trailing edge points are frozen this time, leaving 13 design variables, 12 geometric plus the angle of attack. For the regular fixed thickness constraint cases used for comparison, only one thickness constraint is used:  $t/c \geq 0.1206$  at  $x/c = 0.35$ , and at  $x/c = 0.45$  in a second case. The conditions for the 4-point cases are described later.

For the area constraint case, the target area  $A^*$  is simply the initial area of the RAE 2822 airfoil. No other constraints are used. A weighting of  $\omega_P=1000$  is used to ensure the final area is close to the target area; lower values in this case resulted in much smaller areas, making a fair comparison to the other cases problematic. Finally, for the floating thickness constraint case, the minimum thickness is set at  $x/c=0.1206$ , to be achieved within  $0.2 \leq x \leq 0.55$ .

The drag coefficient at  $C_L=0.733$  vs.  $M$  is plotted for the final designs in Figure 3.1. The results are predictably bad for anything other than the one design point at  $M=0.76$ . All the solutions have roughly the same drag profiles, with some differences. The  $x/c=0.45$  fixed thickness case yielded virtually the same drag coefficient at  $M=0.76$  as the floating thickness constraint. This is because the latter case settled on  $x/c=0.45$  for its maximum thickness location. The final airfoil shapes for both, shown in Figure 3.1, are also very similar. The  $x/c=0.45$  fixed thickness case achieves a thickness of  $t/c=0.1179$ , compared to  $t/c=0.1173$  for the floating thickness constraint at the same point. The area constraint case, on the other hand, settles on  $x/c=0.38$  for its maximum thickness location, where  $t/c=0.1180$ , close to the other cases. Near the design point, it perform slightly worse than the  $x/c=0.35$  fixed thickness case, but it performs better at lower Mach numbers than all the rest of the cases. These last two cases also have similar airfoil shapes, which is not surprising considering the maximum thickness locations.

The area constraint case achieves 99.97% of the initial (target) area, with the similarly performing  $x/c=0.35$  fixed thickness case achieving 97.8%. The floating thickness case achieves 93.7%, while the  $x/c=0.45$  fixed thickness case reaches a close 92.9%. In fact, the drag coefficient

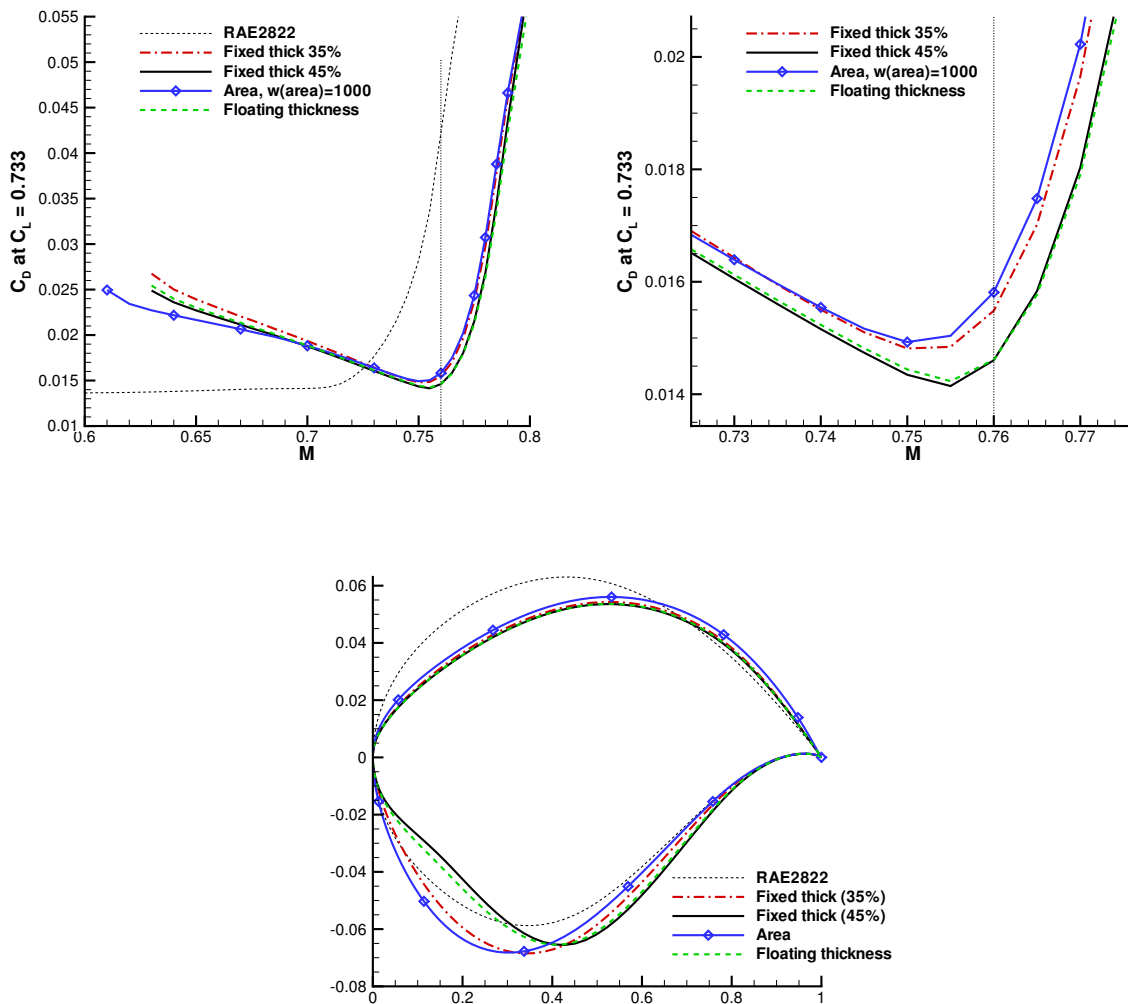


Figure 3.1: Single-point constraint cases.

of the airfoils at  $M=0.76$  rank in the same order as the area of the airfoils: the highest area results in the highest  $C_D$ . If the area constraint case is taken as the baseline, the proportion of drag coefficients is even roughly proportional to the area achieved. The floating thickness case give a drag coefficient 92.4% of the area constraint case, with the  $x/c=0.35$  and  $x/c=0.45$  fixed thickness cases giving 97.9% and 92.36% respectively.

The difference of the single-point area constraint case compared to the others can also be seen in the  $C_P$  graphs in Figures 3.2-3.3. For the area constraint case, the pressure difference is much higher in the middle of the airfoil, similar to the initial RAE 2822 airfoil. The fixed and floating thickness cases all tend to load the leading edge, with little loading in the middle. This can also be seen in the Mach number contour graphs in Figures 3.4-3.6. For comparison,

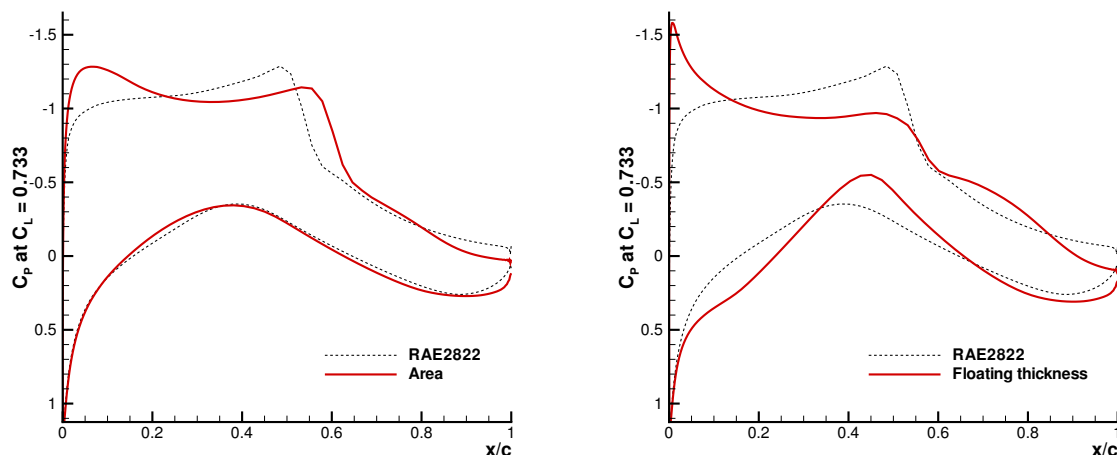


Figure 3.2: Pressure distribution for the single-point alternative constraint cases.

the contour graph for the RAE 2822 airfoil is shown in Figure 3.5. If a more even pressure distribution is desired, the area constraint option may prove more suitable than the others.

The alternative constraints are also tested on a four-point case. Four different Mach number design points are used,  $M=0.68, 0.71, 0.74,$  and  $0.76$ .  $C_L^*=0.733$  and  $C_D^*=0.012$  for all points, at a Reynolds number of 2.7 million. The objective function weights are  $\omega_L=4.0$  and  $\omega_D=1.0$ ; the fixed thickness case uses a constraint weight  $\omega_P=1.0$ , with the following constraints:  $t/c \geq 0.0253$  at  $x/c = 0.01$ ,  $t/c \geq 0.1206$  at  $x/c = 0.35$ ,  $t/c \geq 0.005$  at  $x/c = 0.96$ , and  $t/c \geq 0.0012$  at  $x/c = 0.99$ . The same geometry and parametrization are used, giving 13 design variables. The objective function in such a problem is the weighted sum of the objective functions at each Mach number, as given in Eq. 1.4. The weightings, from lowest Mach number to highest, are: [0.2163 0.2218 0.1904 0.3715].

For the four-point area constraint case,  $\omega_P=1$  and  $\omega_P=10$  were used, in two separate runs. The floating thickness constraint case uses the same constraints as in the single-point case.

The fixed and floating thickness constraint cases, while taking on different final shapes, give almost identical  $C_D$  profiles, as shown in Figure 3.7. The fixed case achieves  $t/c=0.1143$  at  $x/c=0.35$ ; the floating case gives  $t/c=0.1138$ , once again settling on  $x/c=0.35$  for its maximum thickness location.

The 4-point area constraint cases show again the dependence on how much of the target area is achieved. Using  $\omega_P=1$ , the final airfoil's area is only 94% of the initial area, resulting in a reduced maximum thickness of  $t/c=0.1109$  at  $x/c=0.35$ . Its drag coefficient profile, in Figure

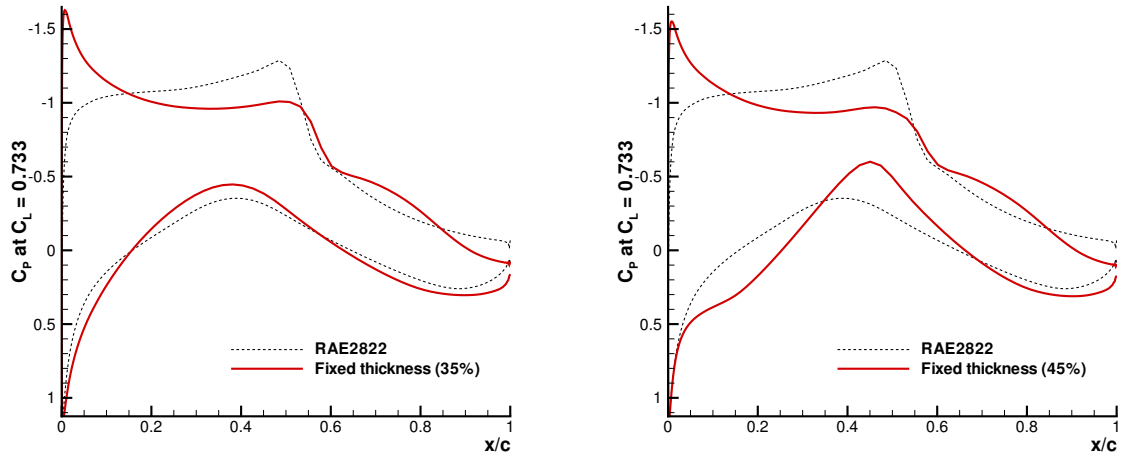
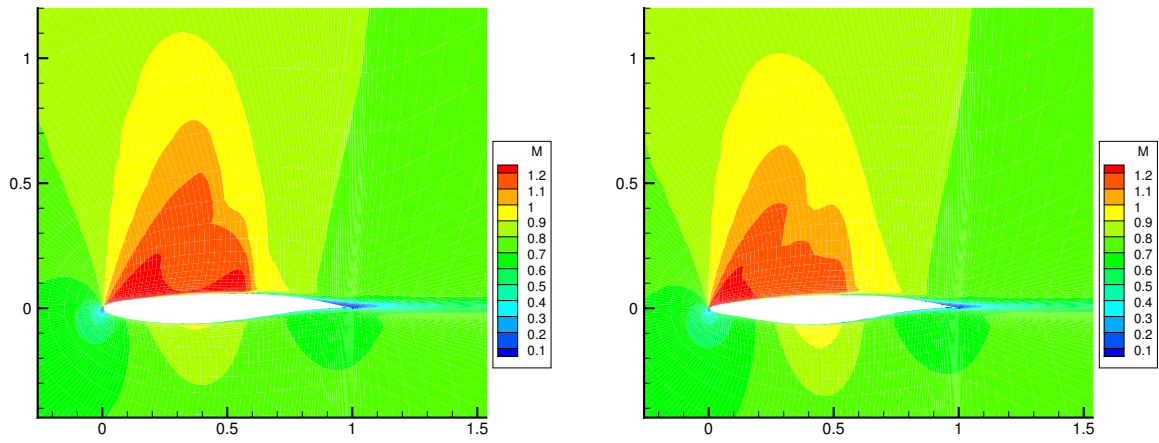


Figure 3.3: Single-point fixed thickness cases,  $C_p$  distribution.



a) Area

b) Floating thickness

Figure 3.4: Mach number contour graphs for the single-point area and floating thickness constraint cases.

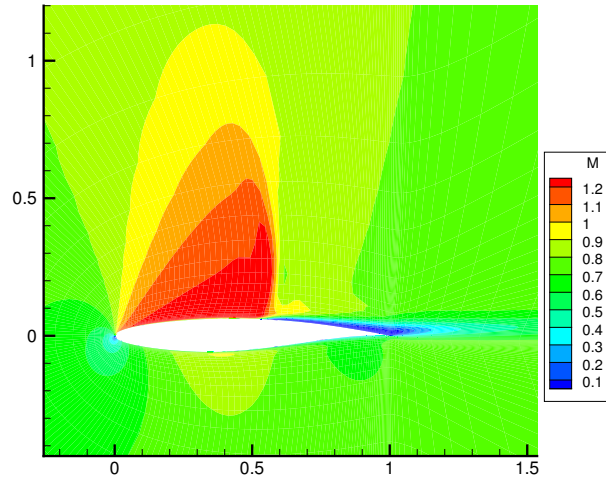
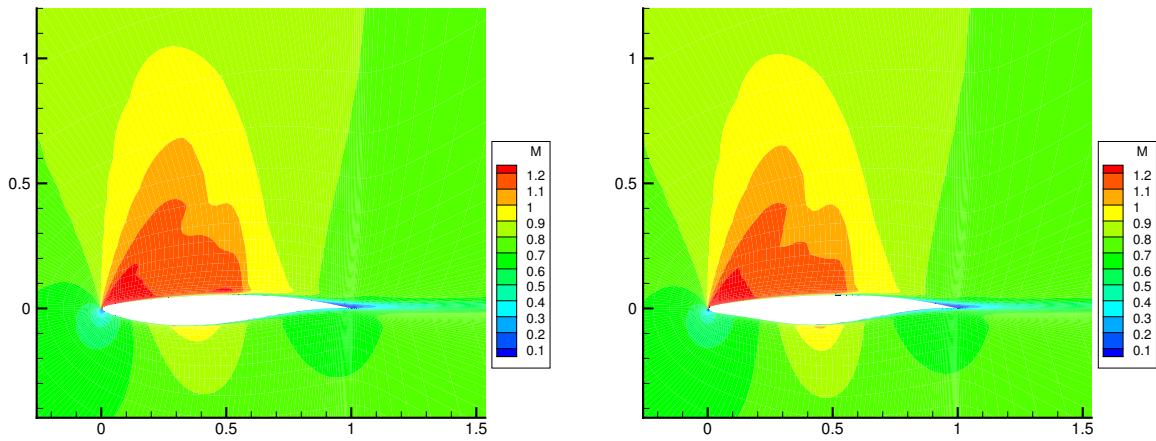


Figure 3.5: Initial airfoil RAE2822 at  $M = 76$ ,  $C_L = 733$



a) Fixed  $.35c$

b) Fixed  $.45c$

Figure 3.6: Mach number contour graphs for the single-point fixed thickness cases.

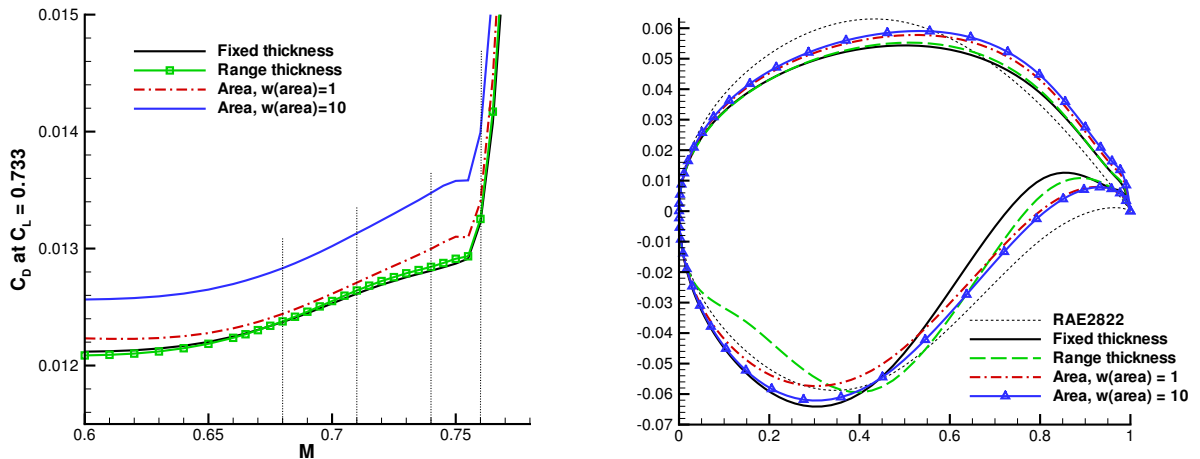


Figure 3.7: Mach number/drag sweeps and airfoils for the 4-point constraint cases.

3.7, comes close to the previous two cases, but performs slightly worse, especially at  $M=0.76$ . When  $\omega_P=10$  is used, the thickness is closer to the first two cases,  $t/c=0.1166$  at  $x/c=0.35$ , but the drag coefficient profile is noticeably worse across all Mach numbers, on average about 4% higher. The reason for this may be the noticeably thicker trailing section, between  $0.6c$  and  $0.9c$ . The fixed thickness case achieved 89.7% of the original area, and the floating thickness achieves 88.9%. Both have similar drag profiles, lower than the area constraint cases, which achieve higher airfoil areas.

As in the single-point cases, the pressure distributions for the area constraint cases, shown in Figure 3.8, have higher loading in the mid-section than the other two cases. The fixed and floating thickness constraint cases display a larger lower surface near-supersonic Mach number bulge. All the four-point cases, however, significantly reduce the leading edge shock wave in the initial RAE 2822 airfoil (Figure 3.5).

Both alternative constraints show advantages. The floating thickness constraint in these cases did not cost the design in performance, doing just as well in the drag coefficient sweeps as the fixed constraint cases. This could be offset by a slightly more problematic shape, as in the four-point case, but with proper problem formulation this disadvantage can probably be minimized or eliminated, while allowing greater flexibility in the optimization process. The area constraint also seems to show some advantage in producing a more even loading across the airfoil, should this be a desirable feature. However, as shown in the four-point case, this can come at a cost to performance in some cases, due to the focus on keeping the original area; other constraint methods may achieve a solution with lower drag primarily because they also result in airfoils

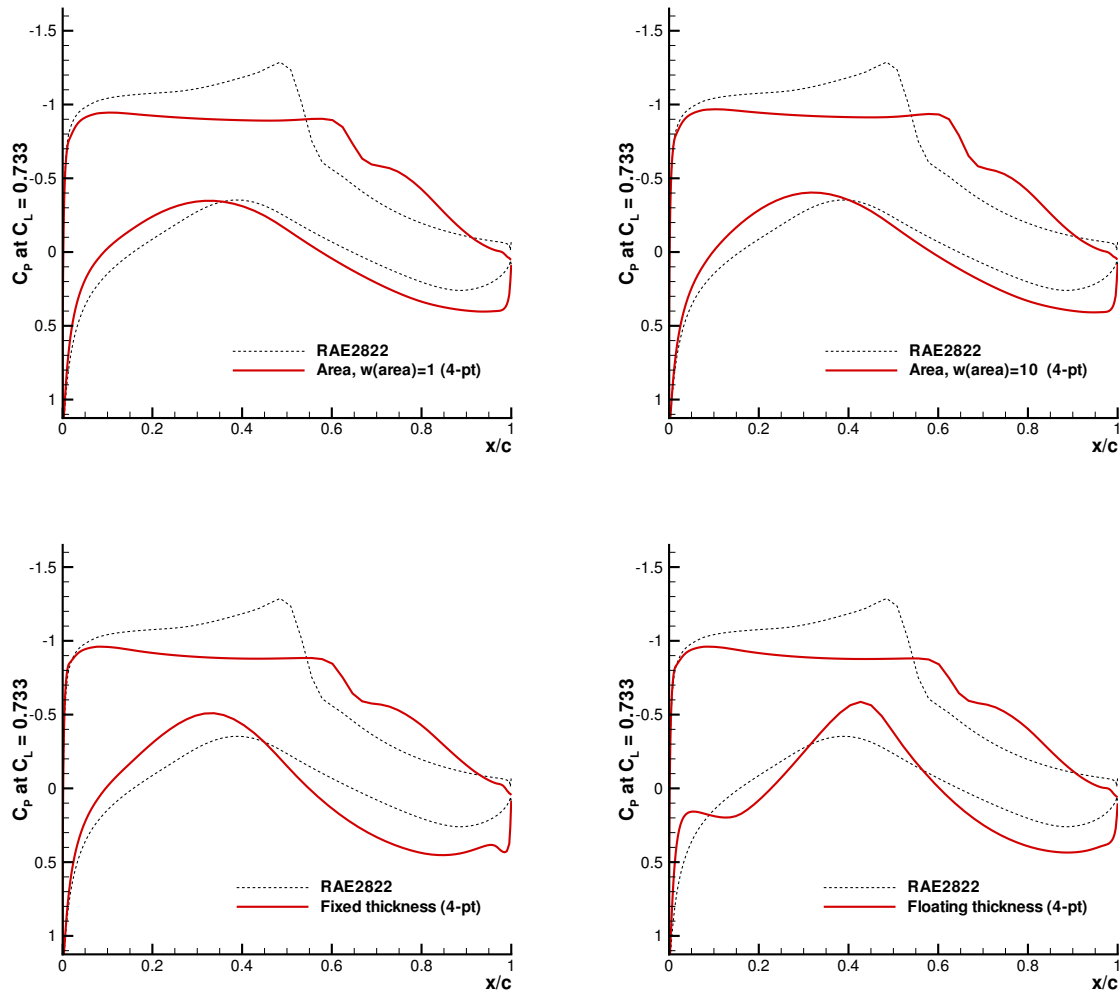


Figure 3.8:  $C_P$  distribution for the 4-point constraint cases at  $M=0.76$ .

with smaller areas. Each can have its uses in allowing more flexibility in the formulation of a design problem, when thickness constraints are not necessarily strict in their placement.

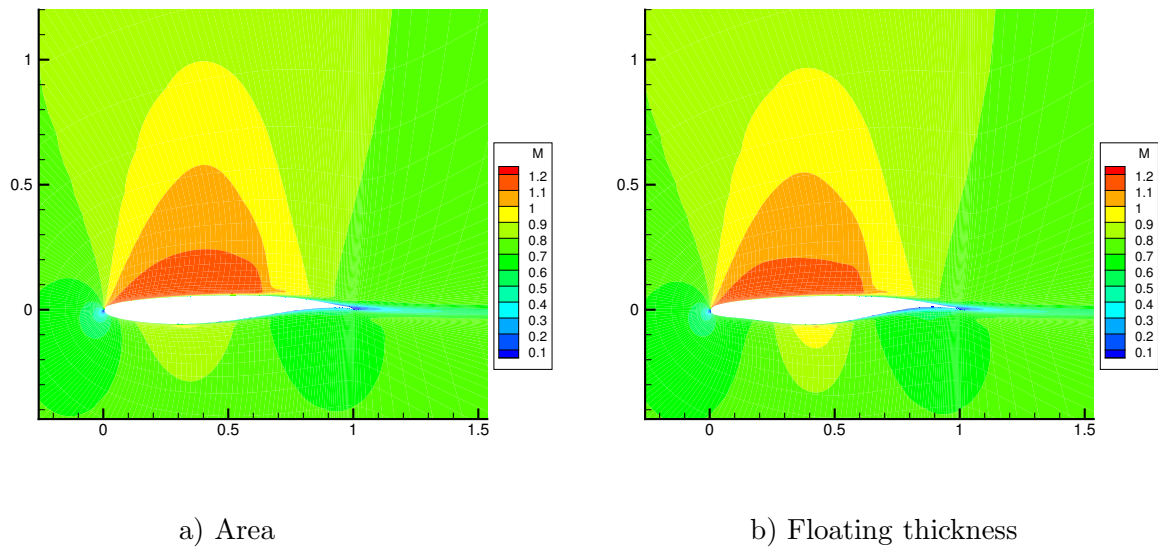


Figure 3.9: Mach number contour graph for the 4-point area and floating thickness constraint cases, at  $M=0.76$  and  $C_L=0.733$ .

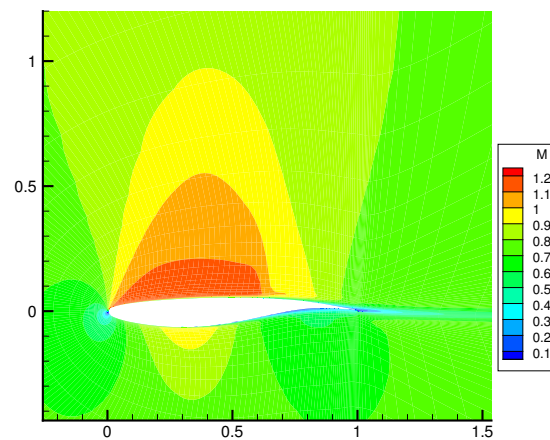


Figure 3.10: Mach number contour graph for the 4-point fixed thickness case, at  $M=0.76$  and  $C_L=0.733$ .



## Chapter 4

# Automatic Weighting Technique

### 4.1 Method

One of the many factors confronting a designer are the multitude of weighting factors that needed to be decided. Often the usual method is to make educated guesses about the weightings needed, making corrections through trial and error. However, it can be advantageous to remove the designer input from the weighting of multi-point objectives, allowing an automated process to adjust the weights according to a formula, iteratively correcting the weights to redirect the design towards a certain objective.

The objective chosen to attempt this is to minimize as well as equalize the drag coefficients of an airfoil across a broad Mach number range. This is mostly an arbitrary objective; while it may be disadvantageous in most cases to equalize  $C_D$  over several Mach numbers, the method described here can be modified to drive the solution towards a different proportional distribution of the drag coefficient profile.

Since any deviation from an equal  $C_D$  profile needs to be corrected by the optimization process, a greater weighting needs to be assigned to the deviated design points after an iteration, in order to attempt to rectify the design in the next iteration. Therefore, the following formula is used to calculate the weights for the next optimization run, or iteration:

$$w_i^{new} = w_i^{old} + c \left( \frac{C_{Di}}{\sum_{i=1}^N C_{Di}} - \frac{1}{N} \right) \quad (4.1)$$

where  $N$  is the number of sampling points, and  $c$  is a user-specified constant. If  $w_i^{new}$  is negative,

it is set to zero. Since the resulting sum of the remaining weights in this case will not be unity, the difference of the total is divided and added equally to all remaining weights. (Note that each iteration is a full optimization run. This should not be confused with the quasi-Newton or line search iterations within an optimization run.)

Depending on the value of  $c$ , this method can vary some weights constantly, which can prove problematic. An attempt to alleviate this while maintaining an aggressive  $c$  led to a second possible method. The basic formula is the same as Eq. 4.1, except that the weight is only changed if the  $C_D$  exceeds the standard deviation of the  $C_D$  at all the sampling points. Weight sets that do not add up to one are tweaked as mentioned earlier. This will be called the standard deviation method, as opposed to the automated weights method.

Along with drag deviations at the design points, there can be unexpected deviations at other Mach numbers, as a result of undesirable trade-offs between design and off-design points. Therefore, additional design points can be automatically added at any significant local maxima in order to achieve a drag coefficient reduction across a broad range of Mach numbers.

## 4.2 Results

The automated weights method is tested on a 4-point multiple Mach number design (although this turns into a 5-point problem as shown below). The initial Mach numbers for the design points are  $M = 0.68, 0.70667, 0.73333, \text{ and } 0.76$ , an even distribution between 0.68 and 0.76. Initially the design point weightings  $w_i = [0.25 \ 0.25 \ 0.25 \ 0.25]$ . The targets are  $C_L^* = 0.733$  and  $C_D^* = 0.01$ , with  $\omega_L = 1.0, \omega_D = 0.1, \omega_P = 1.0$ , and a Reynolds number of 9 million. The following thickness constraints are used:  $t/c \geq 0.0253$  at  $x/c = 0.01$ ,  $t/c \geq 0.121$  at  $x/c = 0.35$ ,  $t/c \geq 0.0137$  at  $x/c = 0.924$ , and  $t/c \geq 0.001516$  at  $x/c = 0.99$ . The first thickness constraint prevents a sharp leading edge from developing (an alternate method to simply freezing the leading three control points).

Case 1 uses the above general conditions, with the same initial geometry as before, an RAE 2822 airfoil with 13 design variables, and a  $c$  value of 30. Tables 4.1-4.2 show the progression of the weights, drag coefficients, standard deviation of  $C_D$ , maximum and minimum  $C_D$ , and  $C_D$  range for each iteration. The standard deviation and range of  $C_D$  is reduced with each successive iteration, with a few exceptions. At the ninth iteration the weighting of the second design point falls to zero. This means that  $C_D$  at this point has dropped so low that it actually needs to rise to be equalized. Due to the formulation of the objective function in Eq. 1.3, the way to do this is to drop the design point and let the solution naturally sacrifice drag reductions

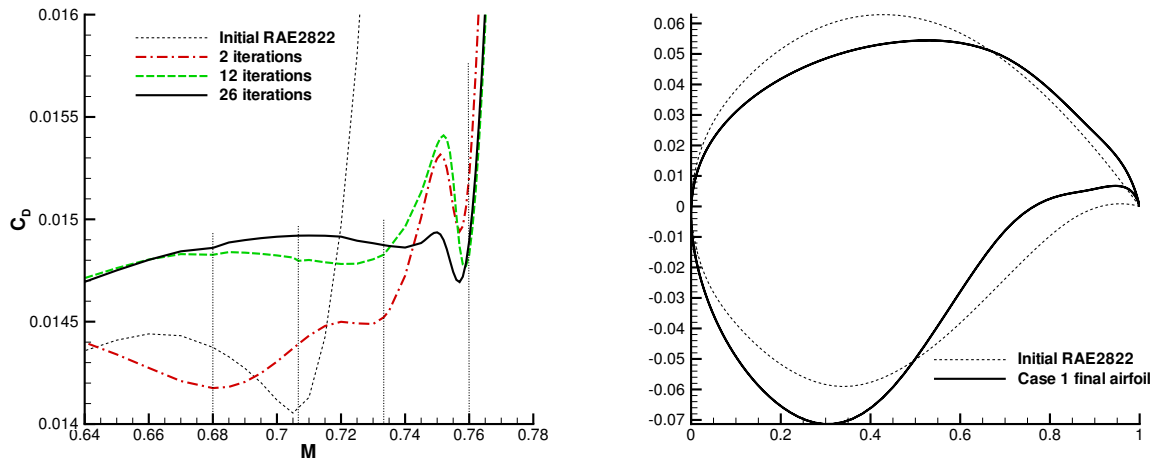


Figure 4.1: Case 1, 13 design variables,  $c = 30$ ; Mach number/drag sweeps and airfoil

at that point to lower the drag at other Mach numbers.

While the  $C_D$  values do start to equalize in Table 4.2, it quickly becomes clear that the drag coefficient at  $M=0.752$  is not being reduced along with its neighbouring design points; the desired equal drag over a broad Mach number range is not being accomplished. When the original four design points have equalized drag to within  $3.0 \times 10^{-5}$  with a standard deviation of  $1.44 \times 10^{-5}$ , a fifth point is added at the local  $C_D$  maximum at  $M=0.752$ . Once this point is included in the optimization problem as of iteration 13, the weight is adjusted accordingly from 0 to 0.175766. After this point the 5-point problem proceeds as the 4-point problem did before. The second design point at  $M=0.70667$  is reactivated as its  $C_D$  rises high enough to raise its weight above zero.

The  $C_D$  sweeps for various iterations of Case 1 are shown in Figure 4.1, as well as the final airfoil shape. This demonstrates dramatically how the drag coefficient for the lower Mach numbers was in fact raised in order to equalize  $C_D$  for all the design points, with a corresponding decrease in the drag coefficient at the higher Mach numbers (the more difficult design points). Once again it should be mentioned that equalizing the drag profile is an arbitrary design objective; nonetheless, the effect shows that the automated weight formula does achieve its intended purpose. Note the dip in  $C_D$  around  $M=0.755$ , just before rising at  $M=0.76$ .  $C_P$  distributions and the Mach number contour graph for the design points are shown in Figures 4.2 and 4.3. They show the familiar narrowing in the mid-section, as well as the lower surface Mach number bulge comparable to the previous design examples.

Table 4.1: Weights for Case 1: 13 DV,  $c = 30$ 

	c	Weights (Mach No.)				
		0.68	0.70667	0.7333	0.752	0.76
1		0.250000	0.250000	0.250000		0.250000
2	30	0.120334	0.142760	0.261765		0.475141
3	30	0.067041	0.088363	0.273654		0.570942
4	30	0.106160	0.069881	0.231428		0.592531
5	30	0.095931	0.044117	0.234324		0.625628
6	30	0.117640	0.032004	0.219701		0.630654
7	30	0.114569	0.016515	0.226941		0.641976
8	30	0.127650	0.007144	0.223945		0.641261
9	30	0.130507	0.000000	0.228886		0.640606
10	30	0.129885	0.000000	0.230511		0.639604
11	30	0.130382	0.000000	0.230943		0.638675
12	30	0.130647	0.000000	0.230943	0.000000	0.638675
13	30	0.072119	0.000000	0.172499	0.175766	0.579616
14	30	0.182337	0.049099	0.113351	0.138609	0.516604
15	30	0.090059	0.016557	0.132988	0.205503	0.554893
16	30	0.132930	0.048126	0.109179	0.178950	0.530815
17	30	0.083416	0.040523	0.118175	0.203831	0.554056
18	30	0.113410	0.066985	0.099436	0.184570	0.535599
19	30	0.073779	0.063363	0.104617	0.204409	0.553832
20	30	0.090547	0.084214	0.090206	0.191643	0.543390
21	30	0.067512	0.087726	0.089605	0.202761	0.552395
22	30	0.077646	0.105856	0.078051	0.194173	0.544274
23	30	0.055519	0.109378	0.076721	0.205231	0.553151
24	30	0.063264	0.126137	0.065461	0.199387	0.545752
25	30	0.048599	0.132865	0.061611	0.206215	0.550710
26	30	0.047381	0.146111	0.053999	0.204023	0.548486

Table 4.2: Results for Case 1: 13 DV,  $c = 30$ 

	$C_D$ ( $C_L=0.733$ )					Max $C_D$	Min $C_D$	St Dev	$C_D$ range
	0.68	0.70667	0.7333	0.752	0.76				
1	0.014484	0.014528	0.014762		0.015181	0.015181	0.014484	0.0003192	0.000697
2	0.014639	0.014637	0.014767		0.014932	0.014932	0.014637	0.0001396	0.000295
3	0.014901	0.014787	0.014740		0.014866	0.014901	0.014740	0.0000733	0.000161
4	0.014768	0.014737	0.014794		0.014853	0.014853	0.014737	0.0000493	0.000116
5	0.014865	0.014798	0.014793		0.014832	0.014865	0.014793	0.0000334	0.000072
6	0.014803	0.014779	0.014824		0.014832	0.014832	0.014779	0.0000236	0.000053
7	0.014851	0.014806	0.014819		0.014824	0.014851	0.014806	0.0000187	0.000044
8	0.014830	0.014802	0.014834		0.014823	0.014834	0.014802	0.0000142	0.000032
9	0.014825	0.014798	0.014830		0.014825	0.014830	0.014798	0.0000143	0.000032
10	0.014828	0.014799	0.014828		0.014825	0.014828	0.014799	0.0000142	0.000029
11	0.014827	0.014798	0.014827		0.014825	0.014827	0.014798	0.0000144	0.000030
12	0.014827	0.014797	0.014827	0.015410	0.014825	0.015410	0.014797	0.0002646	0.000613
13	0.015272	0.015119	0.014848	0.014903	0.014839	0.015272	0.014839	0.0001912	0.000433
14	0.014620	0.014768	0.014897	0.015014	0.014943	0.015014	0.014620	0.0001560	0.000394
15	0.015046	0.015018	0.014880	0.014873	0.014880	0.015046	0.014873	0.0000852	0.000173
16	0.014737	0.014841	0.014882	0.014922	0.014918	0.014922	0.014737	0.0000758	0.000184
17	0.015004	0.014996	0.014883	0.014882	0.014884	0.015004	0.014882	0.0000642	0.000123
18	0.014768	0.014857	0.014879	0.014915	0.014911	0.014915	0.014768	0.0000599	0.000147
19	0.014959	0.014969	0.014882	0.014886	0.014891	0.014969	0.014882	0.0000430	0.000088
20	0.014821	0.014887	0.014877	0.014906	0.014901	0.014906	0.014821	0.0000339	0.000085
21	0.014934	0.014954	0.014880	0.014888	0.014889	0.014954	0.014880	0.0000330	0.000074
22	0.014824	0.014887	0.014875	0.014906	0.014900	0.014906	0.014824	0.0000329	0.000082
23	0.014921	0.014944	0.014874	0.014887	0.014884	0.014944	0.014874	0.0000293	0.000070
24	0.014848	0.014901	0.014875	0.014902	0.014897	0.014902	0.014848	0.0000231	0.000053
25	0.014897	0.014933	0.014881	0.014895	0.014894	0.014933	0.014881	0.0000194	0.000052
26	0.014861	0.014908	0.014874	0.014899	0.014894	0.014908	0.014861	0.0000194	0.000047

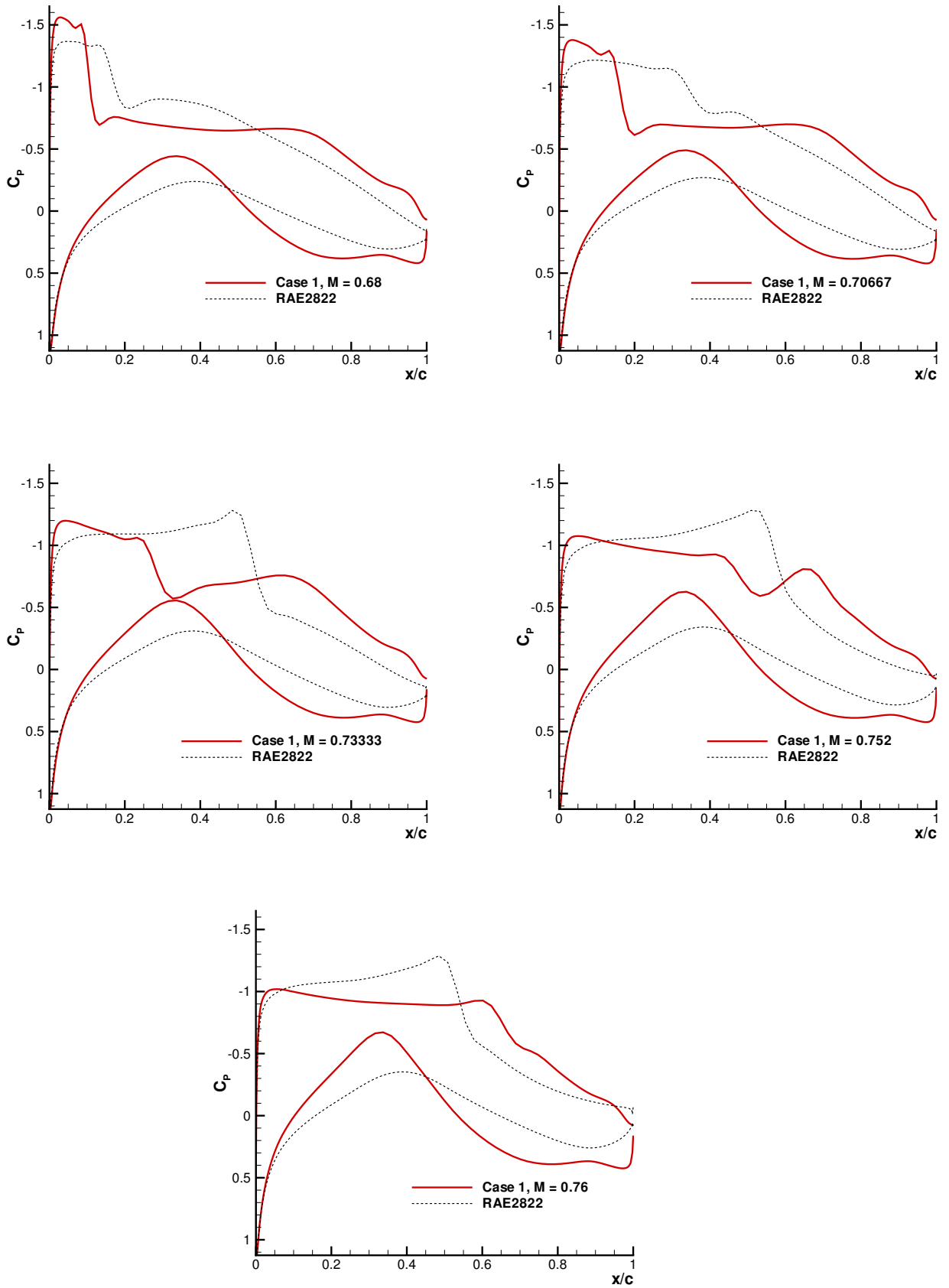


Figure 4.2: Case 1,  $C_p$  graphs for all five design points, for  $C_l = 0.733$  .

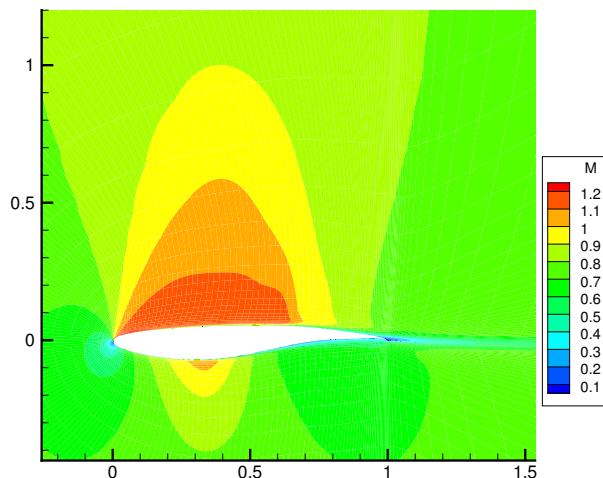
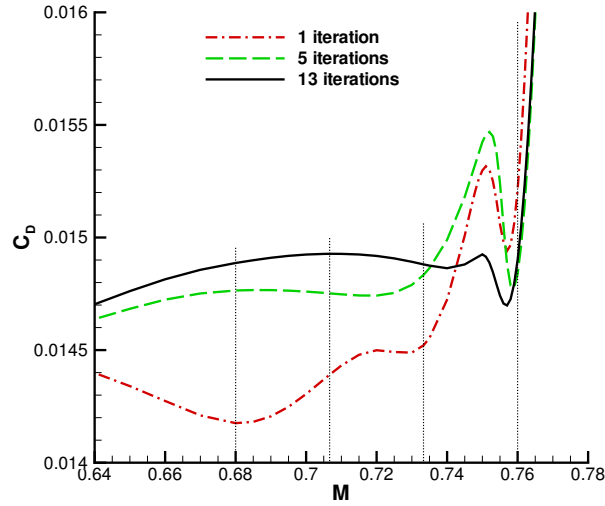


Figure 4.3: Case 1, 13 DV,  $c = 30$ ; Mach number contour graph at  $M=0.76$ ,  $C_L=0.733$ .

Case 2 uses the same conditions as Case 1, but the standard deviation method is used instead of the plain automated weights formula. The data for this run are listed in Tables 4.3-4.4. In this case, the fifth design point is added much sooner. However, even accounting for this, the 5-point problem then proceeds towards the same standard deviation of  $C_D$  as Case 1 in fewer iterations, 7 as opposed to 13. It is also notable that, due to the stabilising effect on the weights of only changing the weights when the  $C_D$  at a point exceeds the standard deviation, a design point is only dropped for one iteration (the 8th).  $C_D$  is plotted vs.  $M$  in Figure 4.4. It is virtually the same solution as Case 1.

Case 3 also uses the standard deviation method, but the cut-off is half the standard deviation,  $0.5\sigma$ , instead of simply  $\sigma$ . The second design point drops out for one iteration, the 8th (Table 4.5). The standard deviation of  $C_D$  is reduced faster than in Case 1, but slower than Case 2 (Table 4.6). Figure 4.5 shows the familiar drag profile for this case.

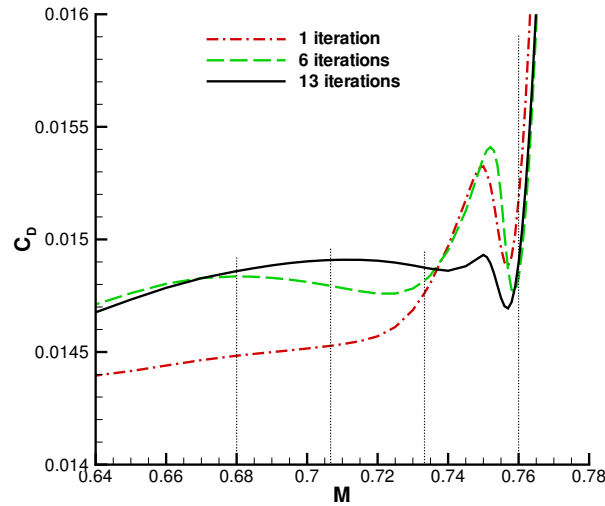
Figure 4.6 shows the standard deviation and maximum  $C_D$  plotted vs. iterations for Cases 1-3. The large spikes in the graph are from the addition of the fifth design point at  $M=0.752$ . Since the fifth point is not consistently added after reaching the same standard deviation, it is more instructive to look at the progress made after the large jumps. From these, it is obvious that using  $c = 30$  without mitigating it with the standard deviation method causes oscillation in the maximum  $C_D$ , which likely makes it slower to converge to a smaller standard deviation. Even using  $\sigma$  as a cut-off instead of  $0.5\sigma$  makes a difference, as Case 2 displays one major oscillation at iteration 8.

Figure 4.4: Case 2, 13 DV,  $c = 30$ , standard deviation method; Mach number/drag sweepsTable 4.3: Weights for Case 2: 13 DV,  $c = 15$ , Standard Deviation method

	c	Weights (Mach No.)				
		0.68	0.70667	0.7333	0.752	0.76
1		0.250000	0.250000	0.250000		0.250000
2	30	0.174953	0.174953	0.174953		0.475141
3	30	0.070732	0.169985	0.169985		0.589299
4	30	0.059115	0.158368	0.158368		0.624150
5	30	0.066749	0.135466	0.166002	0.000000	0.631784
6	30	0.012778	0.081496	0.112032	0.215881	0.577814
7	30	0.012778	0.081496	0.112032	0.215881	0.577814
8	30	0.000000	0.084690	0.115226	0.219075	0.581008
9	30	0.206683	0.033019	0.063555	0.167404	0.529337
10	30	0.195756	0.022092	0.052628	0.211114	0.518410
11	30	0.197052	0.023388	0.029474	0.212410	0.537676
12	30	0.200827	0.027163	0.014373	0.216186	0.541451
<b>13</b>	<b>30</b>	<b>0.190857</b>	<b>0.032064</b>	<b>0.004710</b>	<b>0.221086</b>	<b>0.551284</b>
14	30	0.187740	0.044530	0.001593	0.217970	0.548167

Table 4.4: Results for Case 2: 13 DV,  $c = 15$ , Standard Deviation method

	$C_D$ ( $C_L=0.733$ )					Max $C_D$	Min $C_D$	St Dev	$C_D$ range
	0.68	0.70667	0.7333	0.752	0.76				
1	0.014484	0.014528	0.014762		0.015181	0.015181	0.014484	0.0003192	0.000697
2	0.014533	0.014602	0.014853		0.014962	0.014962	0.014533	0.0002032	0.000429
3	0.014735	0.014725	0.014837		0.014857	0.014857	0.014725	0.0000683	0.000132
4	0.014783	0.014763	0.014848		0.014839	0.014848	0.014763	0.0000417	0.000085
5	0.014765	0.014752	0.014834	0.015469	0.014839	0.015469	0.014752	0.0003029	0.000717
6	0.015448	0.015230	0.014860	0.014841	0.014820	0.015448	0.014820	0.0002842	0.000628
7	0.014650	0.014834	0.014949	0.014948	0.014923	0.014949	0.014650	0.0001267	0.000298
8	0.015603	0.015315	0.014860	0.014831	0.014807	0.015603	0.014807	0.0003583	0.000796
9	0.014803	0.014814	0.014798	0.014967	0.014911	0.014967	0.014798	0.0000762	0.000169
10	0.014871	0.014877	0.014818	0.014888	0.014923	0.014923	0.014818	0.0000380	0.000105
11	0.014878	0.014901	0.014849	0.014894	0.014909	0.014909	0.014849	0.0000239	0.000061
12	0.014855	0.014894	0.014856	0.014890	0.014904	0.014904	0.014855	0.0000228	0.000049
<b>13</b>	<b>0.014887</b>	<b>0.014928</b>	<b>0.014881</b>	<b>0.014888</b>	<b>0.014900</b>	<b>0.014928</b>	<b>0.014881</b>	<b>0.0000187</b>	<b>0.000047</b>
14	0.014852	0.014902	0.014871	0.014895	0.014899	0.014902	0.014852	0.0000215	0.000050

Figure 4.5: Case 3, 13 DV,  $c = 30$ , half standard deviation method; Mach number/drag sweepsTable 4.5: Weights for Case 3: 13 DV,  $c = 30$ , Half Standard Deviation method

	c	Weights (Mach No.)				
		0.68	0.70667	0.7333	0.752	0.76
1		0.250000	0.250000	0.250000		0.250000
2	30	0.120334	0.142760	0.261765		0.475141
3	30	0.067041	0.088363	0.273654		0.570942
4	30	0.106160	0.069881	0.231428		0.592531
5	30	0.093253	0.062599	0.218520		0.625628
6	30	0.100333	0.046589	0.215513		0.637565
7	30	0.109219	0.034010	0.214459	0.000000	0.642311
8	30	0.059328	0.000000	0.164568	0.183683	0.592420
9	30	0.211512	0.069563	0.095104	0.120218	0.503603
10	30	0.094801	0.024190	0.123220	0.209325	0.548463
11	30	0.122707	0.051657	0.107020	0.186498	0.532118
12	30	0.092641	0.053395	0.108758	0.200200	0.545006
13	30	0.091688	0.067337	0.101201	0.195721	0.544053
14	30	0.080674	0.076188	0.096434	0.199186	0.547518
15	30	0.093971	0.095123	0.083664	0.190460	0.536781

Table 4.6: Results for Case 3: 13 DV,  $c = 30$ , Half Standard Deviation method

	$C_D$ ( $C_L=0.733$ )					Max $C_D$	Min $C_D$	St Dev	$C_D$ range
	0.68	0.70667	0.7333	0.752	0.76				
1	0.014484	0.014528	0.014762		0.015181	0.015181	0.014484	0.0003192	0.000697
2	0.014639	0.014637	0.014767		0.014932	0.014932	0.014637	0.0001396	0.000295
3	0.014901	0.014787	0.014740		0.014866	0.014901	0.014740	0.0000733	0.000161
4	0.014768	0.014737	0.014794		0.014853	0.014853	0.014737	0.0000493	0.000116
5	0.014825	0.014779	0.014805		0.014835	0.014835	0.014779	0.0000244	0.000055
6	0.014836	0.014794	0.014816		0.014828	0.014836	0.014794	0.0000184	0.000042
7	0.014827	0.014795	0.014827	0.015408	0.014826	0.015408	0.014795	0.0002639	0.000613
8	0.015415	0.015208	0.014859	0.014874	0.014811	0.015415	0.014811	0.0002650	0.000604
9	0.014546	0.014723	0.014904	0.015055	0.014946	0.015055	0.014546	0.0002010	0.000509
10	0.014989	0.014988	0.014879	0.014863	0.014879	0.014989	0.014863	0.0000632	0.000126
11	0.014802	0.014879	0.014883	0.014911	0.014909	0.014911	0.014802	0.0000441	0.000109
12	0.014892	0.014929	0.014876	0.014883	0.014892	0.014929	0.014876	0.0000205	0.000053
13	0.014859	0.014909	0.014875	0.014894	0.014896	0.014909	0.014859	0.0000195	0.000049
14	0.014944	0.014958	0.014879	0.014889	0.014884	0.014958	0.014879	0.0000371	0.000079
15	<b>0.014825</b>	<b>0.014867</b>	<b>0.014835</b>	<b>0.014876</b>	<b>0.014912</b>	<b>0.014912</b>	<b>0.014825</b>	<b>0.0000348</b>	<b>0.000087</b>

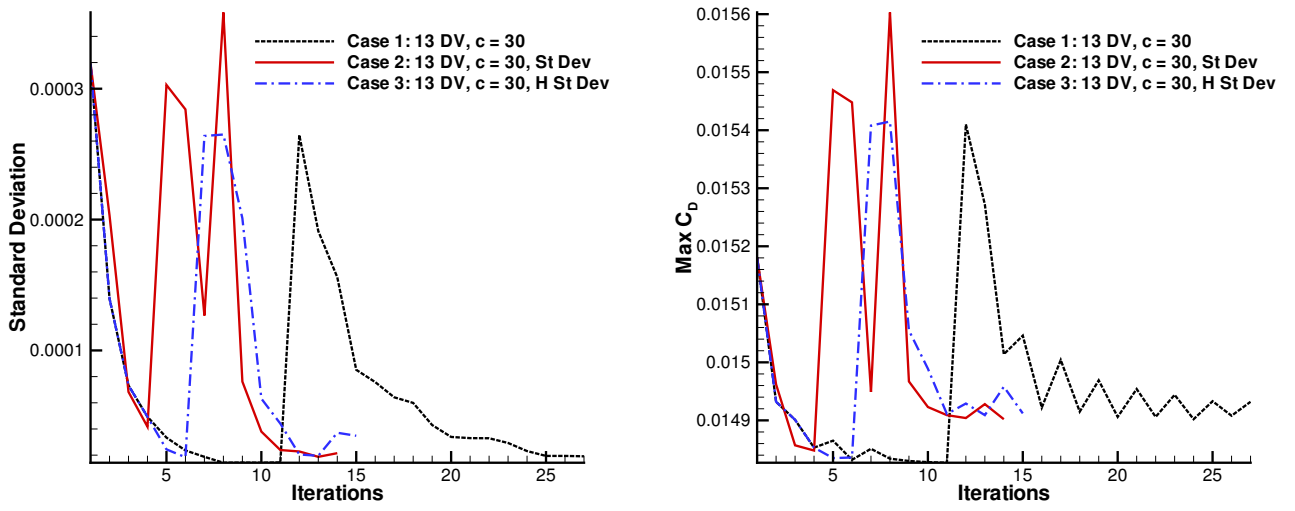


Figure 4.6: Standard deviation of drag and maximum drag at the design points ( $C_L = 0.733$ ) for cases 1-3.

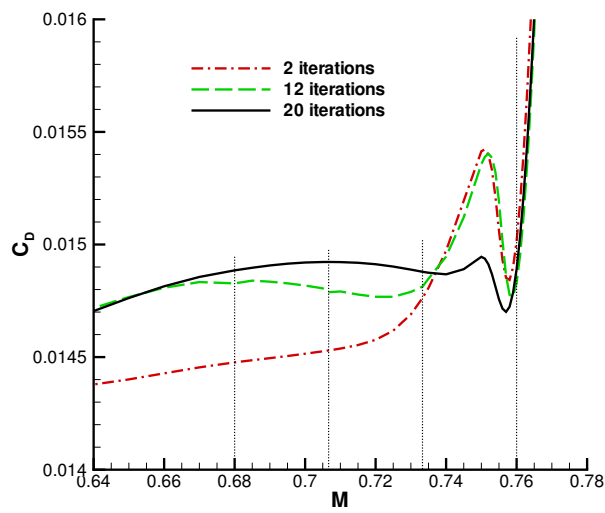


Figure 4.7: Case 4, 13 DV,  $c = 15$ ; Mach number/drag sweeps

Table 4.7: Weights for Case 4: 13 DV,  $c = 15$ 

	c	Weights (Mach No.)				
		0.68	0.70667	0.73333	0.752	0.76
1		0.250000	0.250000	0.250000		0.250000
2	15	0.185167	0.196380	0.255883		0.362571
3	15	0.129128	0.153835	0.272768		0.444269
4	15	0.097432	0.123355	0.279181		0.500031
5	15	0.086286	0.101561	0.274521		0.537632
6	15	0.088032	0.085615	0.263894		0.562459
7	15	0.091966	0.072133	0.253812		0.582089
8	15	0.097655	0.060760	0.245141		0.596444
9	15	0.103324	0.050807	0.238547		0.607323
10	15	0.108992	0.040854	0.231953		0.618201
11	15	0.111648	0.032562	0.230368		0.625422
12	15	0.114774	0.025164	0.229324	0.000000	0.630738
13	15	0.092784	0.000000	0.204430	0.093403	0.609383
14	15	0.116322	0.003727	0.178253	0.117198	0.584500
15	15	0.117652	0.002795	0.165660	0.140850	0.573043
16	15	0.121049	0.005856	0.155519	0.154177	0.563398
17	15	0.119542	0.008486	0.148663	0.165163	0.558145
18	15	0.118187	0.012306	0.142821	0.172836	0.553850
19	15	0.117119	0.017163	0.137857	0.177421	0.550440
20	15	0.114678	0.021898	0.133787	0.181224	0.548414
<b>21</b>	<b>15</b>	<b>0.112122</b>	<b>0.026864</b>	<b>0.129975</b>	<b>0.184043</b>	<b>0.546996</b>

Table 4.8: Results for Case 4: 13 DV,  $c = 15$ 

	$C_D$ ( $C_L=0.733$ )					Max $C_D$	Min $C_D$	St Dev	$C_D$ range
	0.68	0.70667	0.73333	0.752	0.76				
1	0.014484	0.014528	0.014762		0.015181	0.015181	0.014484	0.0003192	0.000697
2	0.014477	0.014529	0.014762		0.015016	0.015016	0.014477	0.0002469	0.000540
3	0.014609	0.014614	0.014759		0.014953	0.014953	0.014609	0.0001617	0.000344
4	0.014721	0.014679	0.014746		0.014913	0.014913	0.014679	0.0001025	0.000234
5	0.014797	0.014727	0.014748		0.014888	0.014888	0.014727	0.0000715	0.000161
6	0.014814	0.014745	0.014759		0.014876	0.014876	0.014745	0.0000596	0.000131
7	0.014820	0.014753	0.014764		0.014855	0.014855	0.014753	0.0000480	0.000102
8	0.014836	0.014774	0.014788		0.014857	0.014857	0.014774	0.0000390	0.000082
9	0.014836	0.014774	0.014788		0.014857	0.014857	0.014774	0.0000390	0.000082
10	0.014829	0.014786	0.014812		0.014847	0.014847	0.014786	0.0000261	0.000061
11	0.014825	0.014783	0.014808		0.014833	0.014833	0.014783	0.0000221	0.000050
12	0.014827	0.014788	0.014813	0.015402	0.014831	0.015402	0.014788	0.0002630	0.000614
13	0.015062	0.014963	0.014814	0.015063	0.014821	0.015063	0.014814	0.0001230	0.000249
14	0.014913	0.014901	0.014843	0.015024	0.014849	0.015024	0.014843	0.0000725	0.000180
15	0.014923	0.014921	0.014856	0.014972	0.014858	0.014972	0.014856	0.0000493	0.000117
16	0.014889	0.014910	0.014863	0.014951	0.014870	0.014951	0.014863	0.0000355	0.000089
17	0.014889	0.014915	0.014867	0.014934	0.014875	0.014934	0.014867	0.0000281	0.000067
18	0.014896	0.014925	0.014876	0.014924	0.014884	0.014925	0.014876	0.0000225	0.000049
19	0.014886	0.014922	0.014878	0.014917	0.014888	0.014922	0.014878	0.0000198	0.000044
20	0.014885	0.014923	0.014879	0.014912	0.014891	0.014923	0.014879	0.0000185	0.000044
<b>21</b>	<b>0.014885</b>	<b>0.014923</b>	<b>0.014879</b>	<b>0.014908</b>	<b>0.014892</b>	<b>0.014923</b>	<b>0.014879</b>	<b>0.0000179</b>	<b>0.000044</b>

Case 4 is the same as Case 1, using the normal automated weight formula, but with  $c = 15$ . In this case, the 4-point section proceeds slower than in Case 1, not reducing the maximum  $C_D$ , standard deviation, or  $C_D$  range as fast (Tables 4.7-4.8). While Case 1 reaches  $\sigma=2.36 \times 10^{-5}$  in 6 iterations, it takes Case 4 eleven iterations to reach  $\sigma=2.21 \times 10^{-5}$ . However once the fifth point is added, Case 4 reaches the same maximum  $C_D$  and a lower standard deviation than Case 1, in 10 instead of 16 iterations. While speed is not the primary goal, it is nonetheless interesting to note. Case 4 also had a point drop out for one iteration; the drag profile is shown in Figure 4.7.

Case 5 uses  $c = 15$  as in Case 4, but uses the half standard deviation method (no weight change unless the  $C_D$  exceeds  $0.5\sigma$ ). The Mach number drag sweeps are shown in Figure 4.8. It

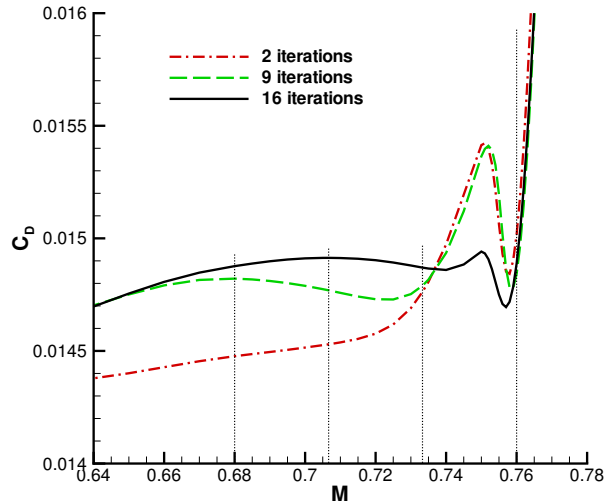


Figure 4.8: Case 5, 13 DV,  $c = 15$ , half standard deviation method; Mach number/drag sweeps reduces the standard deviation slightly faster than Case 4 (Tables 4.9-4.10). Unlike Case 4, no design is ever dropped. For a comparison of the two methods, Figure 4.9 shows little difference between the two. Figure 4.10 does show however that  $c = 15$  is a better choice for avoiding oscillations in the maximum  $C_D$ .

Cases 6 and 7 use a different geometry than the previous cases. The RAE 2822 airfoil is parametrized by a 25-control-point B-spline instead of 15. Freezing the leading and trailing edge points and adding the angle of attack gives 23 design variables. The same thickness constraints are used. For Case 6,  $c = 30$  is used. Looking at Tables 4.11-4.12, the max  $C_D$  and standard deviation fluctuate, sometimes considerably, going from low (3rd iteration) to high (10th iteration) and suddenly back down (11th iteration). The solution does not proceed towards equalization or minimization at a steady rate, but instead falls sharply and suddenly in the final 3 iterations. In fact,  $c$  had to be reduced to 15 in order to stop the repeating cycle of trading off low Mach number performance for high Mach number performance (note the  $C_D$  values after the fifth design point is added at  $M=0.753$ ). The final iteration does have better characteristics ( $C_D$ , max  $C_D$ ,  $\sigma$ ) than any of the previous cases. The drag coefficients are reduced to just below 0.0148, instead of just below 0.0149; see Figure 4.11 for a comparison of all the cases. The larger number of geometric design variables does give the optimizer more freedom to achieve a better solution (Figure 4.12), but with a too aggressive value of  $c$ , the process is unstable.

Table 4.9: Weights for Case 5: 13 DV,  $c = 15$ , Half Standard Deviation method

	c	Weights (Mach No.)				
		0.68	0.70667	0.73333	0.752	0.76
1		0.250000	0.250000	0.250000		0.250000
2	15	0.185167	0.196380	0.255883		0.362571
3	15	0.129131	0.153830	0.272777		0.444262
4	15	0.097386	0.123172	0.279011		0.500431
5	15	0.089627	0.101462	0.271252		0.537660
6	15	0.089905	0.085131	0.261980		0.562984
7	15	0.093629	0.071739	0.252754		0.581878
8	15	0.098068	0.060174	0.244958		0.596800
9	15	0.103280	0.050156	0.238689	0.000000	0.607875
10	15	0.084192	0.018490	0.211197	0.097334	0.588787
11	15	0.106496	0.019593	0.182335	0.122257	0.569319
12	15	0.106731	0.019829	0.166894	0.144957	0.561589
13	15	0.109806	0.022904	0.154118	0.158241	0.554931
14	15	0.112593	0.025690	0.144115	0.167319	0.550283
15	15	0.112056	0.025154	0.135240	0.177805	0.549746
16	15	<b>0.110316</b>	<b>0.029497</b>	<b>0.130178</b>	<b>0.182003</b>	<b>0.548006</b>
17	15	0.107411	0.033998	0.125961	0.185326	0.547304

Table 4.10: Results for Case 5: 13 DV,  $c = 15$ , Half Standard Deviation method

	$C_D$ ( $C_L=0.733$ )					Max $C_D$	Min $C_D$	St Dev	$C_D$ range
	0.68	0.70667	0.73333	0.752	0.76				
1	0.014484	0.014528	0.014762		0.015181	0.015181	0.014484	0.0003192	0.000697
2	0.014477	0.014529	0.014762		0.015016	0.015016	0.014477	0.0002469	0.000540
3	0.014609	0.014613	0.014758		0.014954	0.014954	0.014609	0.0001627	0.000345
4	0.014724	0.014680	0.014746		0.014912	0.014912	0.014680	0.0001015	0.000232
5	0.014789	0.014724	0.014752		0.014888	0.014888	0.014724	0.0000718	0.000164
6	0.014815	0.014747	0.014763		0.014874	0.014874	0.014747	0.0000574	0.000127
7	0.014824	0.014761	0.014776		0.014865	0.014865	0.014761	0.0000476	0.000105
8	0.014834	0.014773	0.014788		0.014857	0.014857	0.014773	0.0000388	0.000083
9	0.014821	0.014769	0.014790	0.015411	0.014842	0.015411	0.014769	0.0002722	0.000642
10	0.015043	0.014938	0.014788	0.015056	0.014835	0.015056	0.014788	0.0001202	0.000268
11	0.014911	0.014888	0.014822	0.015011	0.014860	0.015011	0.014822	0.0000713	0.000189
12	0.014921	0.014908	0.014836	0.014966	0.014867	0.014966	0.014836	0.0000501	0.000129
13	0.014910	0.014912	0.014848	0.014942	0.014874	0.014942	0.014848	0.0000368	0.000095
14	0.014889	0.014901	0.014848	0.014944	0.014877	0.014944	0.014848	0.0000351	0.000096
15	0.014882	0.014914	0.014867	0.014913	0.014885	0.014914	0.014867	0.0000205	0.000047
16	<b>0.014877</b>	<b>0.014913</b>	<b>0.014870</b>	<b>0.014908</b>	<b>0.014888</b>	<b>0.014913</b>	<b>0.014870</b>	<b>0.0000189</b>	<b>0.000043</b>
17	0.014880	0.014916	0.014871	0.014903	0.014888	0.014916	0.014871	0.0000181	0.000045

In Case 7  $c = 15$  is used instead, with predictably more stable results as shown in Tables 4.13-4.14. There are no wild fluctuations in  $\sigma$  and the maximum  $C_D$ , as is graphically shown in Figure 4.13. No design points are dropped, and the final solution has lower  $C_D$  values at the design point than all the other cases, and also a lower standard deviation. The airfoil is, of course, not as smooth as the cases with 12 geometric design variables instead of 23; there is a small dent near the leading edge (Figure 4.14). The Mach number contour graph at  $M=0.76$  is shown in Figure 4.15, while  $C_P$  plots are shown for all the design points in Figure 4.16. They are very similar to Case 1 (Figure 4.2), with notable exceptions where the dip in the lower surface occurs near  $x/c=0.1$ .

These cases demonstrate the various sensitivities of the automated weight formula (Eq. 4.1), with or without the standard deviation method variation. However in general the automated weight method has proven very effective at achieving equal drag coefficients across all the design points, even if a drastically off-design fifth point is added to an otherwise equalized set of points.

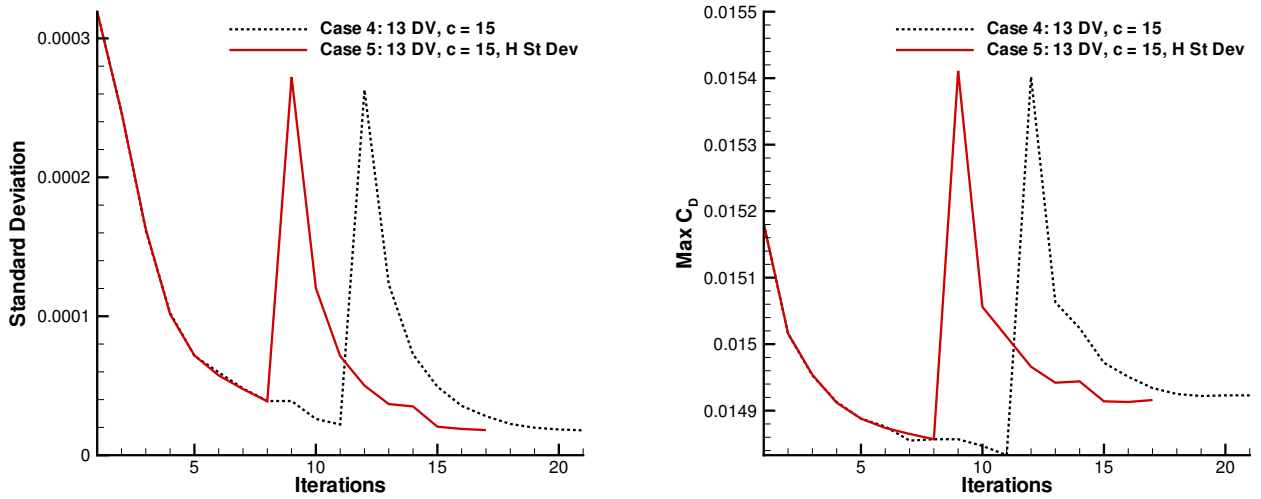


Figure 4.9: Standard deviation of drag and maximum drag at the design points ( $C_L = 0.733$ ) for cases 4 and 5.

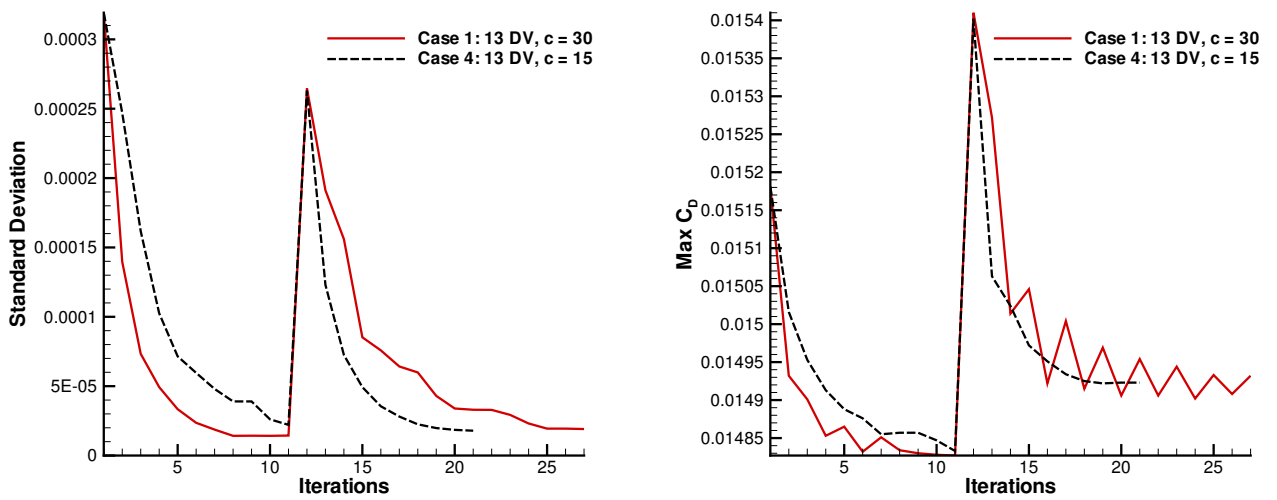


Figure 4.10: Standard deviation of drag and maximum drag at the design points ( $C_L = 0.733$ ) for cases 1 and 4.

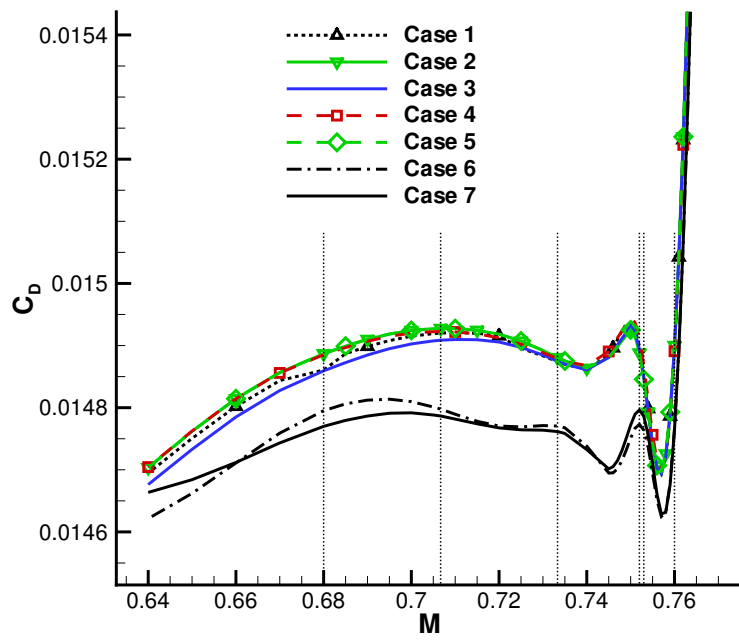


Figure 4.11: Final Mach number/drag sweeps for all automated weight cases.

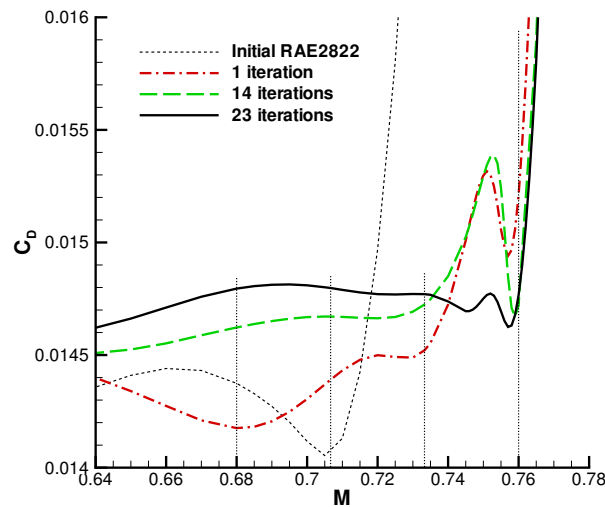


Figure 4.12: Case 6, 23 DV,  $c = 30$ ; Mach number/drag sweeps

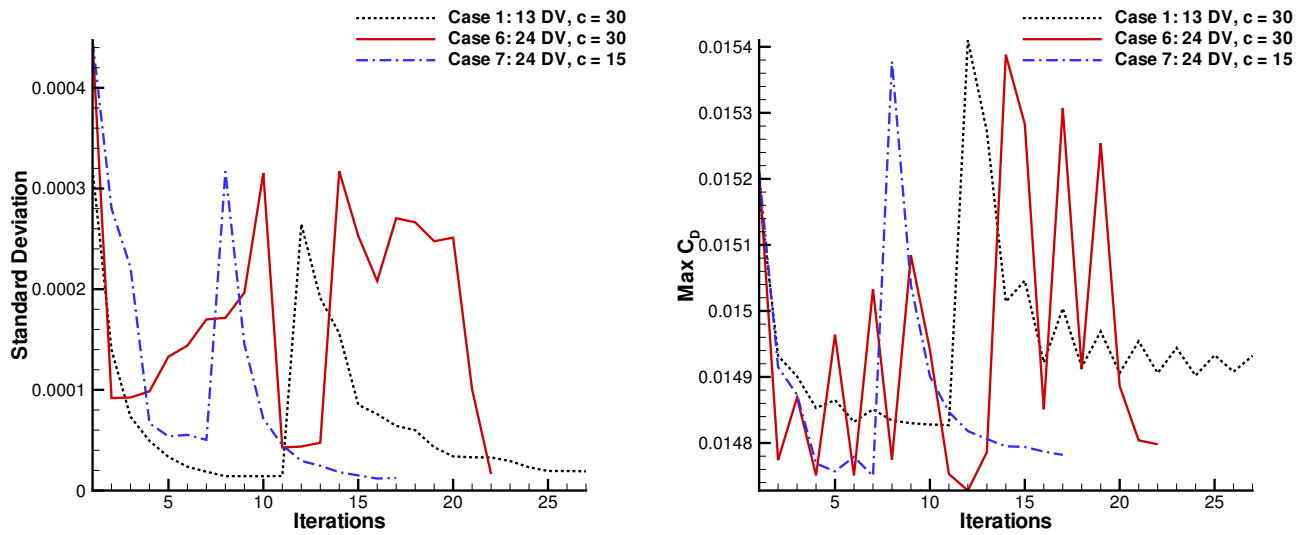


Figure 4.13: Standard deviation of drag and maximum drag at the design points ( $C_L = 0.733$ ) for cases 1, 6 and 7.

This incidentally also demonstrates a rough system for adding design points to smooth out the performance of the airfoil over its Mach number range. Automating this process makes the designer's task of achieving specific drag targets easier and more automated, allowing more attention to be paid to other areas. With modification, the method could potentially be used to optimize for various non-equal  $C_D$  profiles.

Table 4.11: Weights for Case 6: 23 DV,  $c = 30$ 

	c	Weights (Mach No.)				
		0.68	0.70667	0.73333	0.752	0.76
1		0.250000	0.250000	0.250000		0.250000
2	30	0.044710	0.155513	0.222473		0.577303
3	30	0.005889	0.132202	0.217104		0.644806
4	30	0.069464	0.129667	0.167673		0.633196
5	30	0.008927	0.110014	0.194208		0.686851
6	30	0.100336	0.120044	0.137926		0.641694
7	30	0.005055	0.098756	0.195828		0.700360
8	30	0.119023	0.117659	0.124199		0.639119
9	30	0.119023	0.117659	0.124199		0.639119
10	30	0.250460	0.139977	0.042336		0.567227
11	30	0.050011	0.085249	0.207342		0.657398
12	30	0.068398	0.097306	0.176678		0.657617
13	30	0.039252	0.095330	0.183321		0.682096
14	30	0.068750	0.103267	0.156757	0.000000	0.671227
15	30	0.000000	0.037365	0.112563	0.224326	0.625746
16	30	0.152038	0.095906	0.037267	0.164560	0.550229
17	30	0.011143	0.076671	0.085014	0.224708	0.602464
18	30	0.161882	0.152571	0.042655	0.132717	0.510176
19	30	0.000000	0.096754	0.085478	0.229772	0.587996
20	15	0.142935	0.160200	0.043606	0.144453	0.508806
21	15	0.065988	0.133157	0.064559	0.188215	0.548080
22	30	<b>0.033436</b>	<b>0.125945</b>	<b>0.072847</b>	<b>0.203202</b>	<b>0.564569</b>

Table 4.12: Results for Case 6: 23 DV,  $c = 30$ 

	$C_D$ ( $C_L=0.733$ )					Max $C_D$	Min $C_D$	St Dev	$C_D$ range
	0.68	0.70667	0.73333	0.752	0.76				
1	0.014176	0.014391	0.014521		0.015211	0.015211	0.014176	0.0004473	0.001035
2	0.014567	0.014597	0.014632		0.014774	0.014774	0.014567	0.0000918	0.000208
3	0.014869	0.014739	0.014647		0.014721	0.014869	0.014647	0.0000924	0.000222
4	0.014528	0.014608	0.014698		0.014751	0.014751	0.014528	0.0000985	0.000223
5	0.014964	0.014803	0.014673		0.014695	0.014964	0.014673	0.0001330	0.000291
6	0.014450	0.014595	0.014749		0.014751	0.014751	0.014450	0.0001440	0.000300
7	0.015033	0.014846	0.014667		0.014687	0.015033	0.014667	0.0001700	0.000366
8	0.014407	0.014587	0.014775		0.014754	0.014775	0.014407	0.0001715	0.000369
9	0.015084	0.014868	0.014662		0.014682	0.015084	0.014662	0.0001965	0.000422
10	0.014228	0.014512	0.014941		0.014795	0.014941	0.014228	0.0003154	0.000712
11	0.014753	0.014741	0.014657		0.014717	0.014753	0.014657	0.0000427	0.000096
12	0.014623	0.014676	0.014693		0.014728	0.014728	0.014623	0.0000437	0.000105
13	0.014786	0.014743	0.014676		0.014706	0.014786	0.014676	0.0000475	0.000110
14	0.014623	0.014671	0.014725	0.015388	0.014721	0.015388	0.014623	0.0003172	0.000765
15	0.015283	0.015051	0.014719	0.014757	0.014718	0.015283	0.014718	0.0002530	0.000565
16	0.014358	0.014656	0.014820	0.014851	0.014831	0.014851	0.014358	0.0002081	0.000493
17	0.015307	0.015121	0.014827	0.014703	0.014703	0.015307	0.014703	0.0002705	0.000605
18	0.014273	0.014538	0.014779	0.014912	0.014865	0.014912	0.014273	0.0002664	0.000639
19	0.015254	0.015057	0.014795	0.014688	0.014703	0.015254	0.014688	0.0002476	0.000567
20	0.014296	0.014540	0.014775	0.014886	0.014864	0.014886	0.014296	0.0002512	0.000590
21	0.014564	0.014688	0.014764	0.014797	0.014804	0.014804	0.014564	0.0001005	0.000241
22	<b>0.014795</b>	<b>0.014798</b>	<b>0.014770</b>	<b>0.014764</b>	<b>0.014767</b>	<b>0.014798</b>	<b>0.014764</b>	<b>0.0000164</b>	<b>0.000034</b>

Table 4.13: Weights for Case 7: 23 DV,  $c = 15$ 

Iteration	c	Weights (Mach No.)				
		0.68	0.70667	0.73333	0.753	0.76
1		0.25000	0.25000	0.25000		0.25000
2	15	0.14736	0.20276	0.23624		0.41365
3	15	0.07167	0.17371	0.24624		0.50837
4	15	0.01497	0.15141	0.24749		0.58613
5	15	0.01598	0.14456	0.23031		0.60915
6	15	0.02188	0.13996	0.21372		0.62444
7	15	0.03808	0.13543	0.19683		0.62966
8	15	0.04999	0.13010	0.18127	0.00000	0.63865
9	15	0.01311	0.09592	0.15396	0.11384	0.62317
10	15	0.05062	0.10483	0.12189	0.12695	0.59571
11	15	0.04409	0.10294	0.10973	0.15193	0.59131
12	15	0.04441	0.10647	0.09879	0.16495	0.58539
13	15	0.04430	0.11093	0.09259	0.17228	0.57990
14	15	0.04529	0.11475	0.08648	0.17772	0.57576
15	15	0.04622	0.11815	0.08234	0.18116	0.57214
16	15	<b>0.04637</b>	<b>0.12041</b>	<b>0.07901</b>	<b>0.18481</b>	<b>0.56940</b>
17	15	0.04560	0.12302	0.07655	0.18732	0.56751

Table 4.14: Results for Case 7: 23 DV,  $c = 15$ 

	$C_D$ ( $C_L=0.733$ )					Max $C_D$	Min $C_D$	St Dev	$C_D$ range
	0.68	0.70667	0.7333	0.752	0.76				
1	0.014176	0.014391	0.014521		0.015211	0.015211	0.014176	0.0004473	0.001035
2	0.014254	0.014435	0.014586		0.014915	0.014915	0.014254	0.0002801	0.000661
3	0.014351	0.014484	0.014576		0.014873	0.014873	0.014351	0.0002216	0.000522
4	0.014683	0.014652	0.014611		0.014769	0.014769	0.014611	0.0000668	0.000157
5	0.014720	0.014679	0.014632		0.014757	0.014757	0.014632	0.0000538	0.000125
6	0.014779	0.014698	0.014649		0.014736	0.014779	0.014649	0.0000553	0.000130
7	0.014750	0.014682	0.014642		0.014738	0.014750	0.014642	0.0000503	0.000108
8	0.014634	0.014647	0.014681	0.015378	0.014740	0.015378	0.014634	0.0003169	0.000744
9	0.015039	0.014897	0.014694	0.014918	0.014717	0.015039	0.014694	0.0001452	0.000344
10	0.014745	0.014768	0.014718	0.014901	0.014756	0.014901	0.014718	0.0000713	0.000183
11	0.014784	0.014800	0.014729	0.014847	0.014754	0.014847	0.014729	0.0000452	0.000118
12	0.014781	0.014804	0.014751	0.014818	0.014755	0.014818	0.014751	0.0000294	0.000067
13	0.014784	0.014798	0.014749	0.014806	0.014759	0.014806	0.014749	0.0000246	0.000057
14	0.014782	0.014794	0.014757	0.014795	0.014760	0.014795	0.014757	0.0000182	0.000037
15	0.014777	0.014787	0.014760	0.014794	0.014763	0.014794	0.014760	0.0000150	0.000034
16	<b>0.014770</b>	<b>0.014787</b>	<b>0.014762</b>	<b>0.014786</b>	<b>0.014764</b>	<b>0.014787</b>	<b>0.014762</b>	<b>0.0000119</b>	<b>0.000025</b>
17	0.014750	0.014774	0.014761	0.014782	0.014769	0.014782	0.014750	0.0000125	0.000033

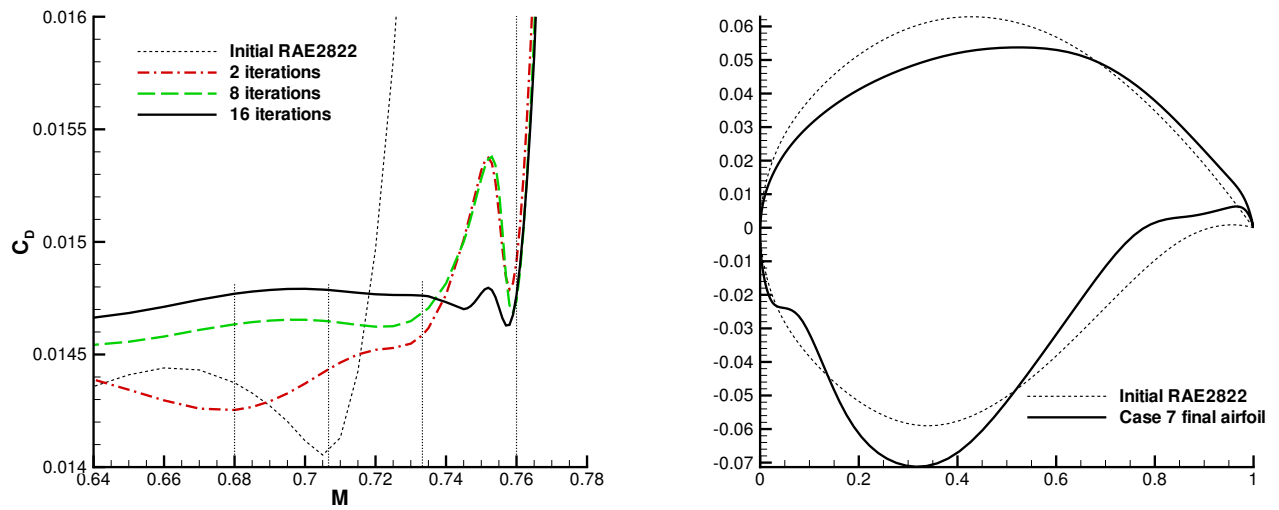


Figure 4.14: Case 7, 23 DV,  $c = 15$ ; Mach number/drag sweeps and airfoil

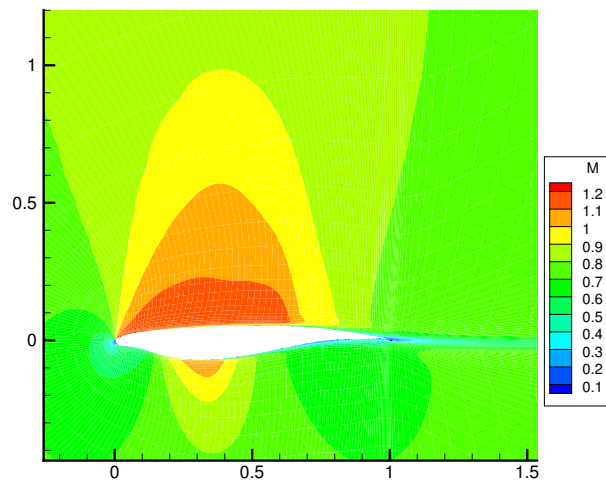


Figure 4.15: Case 7, 23 DV,  $c = 15$ ; Mach number contour graph at  $M=0.76$ ,  $C_L=0.733$ .

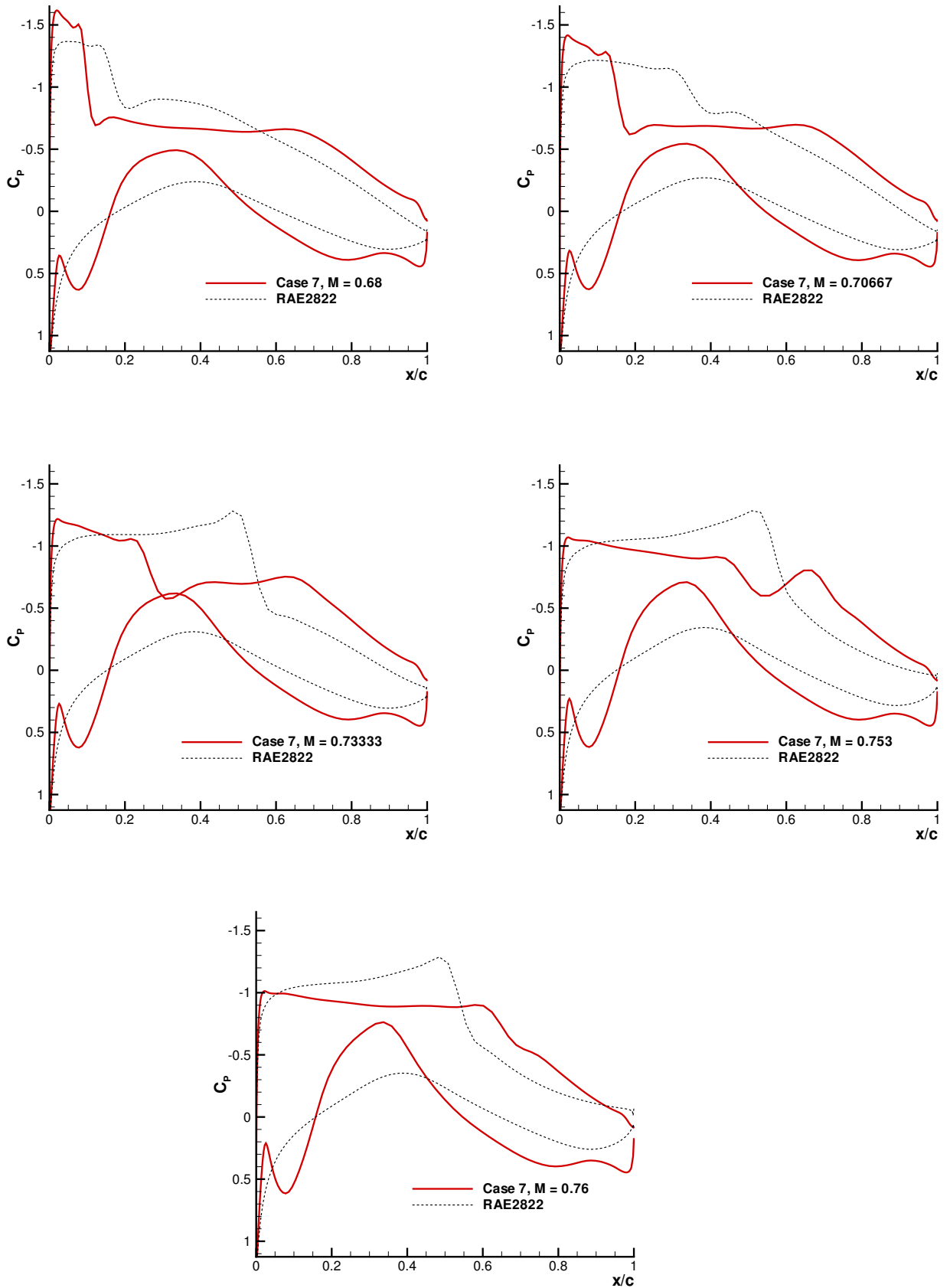


Figure 4.16: Case 7,  $C_p$  graphs for all five design points, for  $C_l = 0.733$ .



## Chapter 5

# Multiple Mach Number and Lift Coefficient Problems

### 5.1 Nine-point General Cases

All the previous multi-point cases have been multiple Mach number cases only, with only the Mach number being different between design points. The one exception is the first Pareto front case, which varied only the  $C_L$  target. However, since airfoils have to be designed for a variety of conditions, it is useful to consider the problem of a case with design points that have both different Mach number and  $C_L^*$ , as well as having even more design points. A properly specified problem that takes into account all the various flying conditions and requirements will involve many design points; therefore this type of problem needs to be explored.

For these multiple Mach number and  $C_L^*$ -varying problems, there are nine design points. For the first case, three freestream Mach number conditions,  $M=0.68$ ,  $0.73$ , and  $0.76$ , are combined with three lift coefficient targets,  $C_L^*=0.65$ ,  $0.733$ , and  $0.77$  in each possible combination, with  $C_D^*=0.01$ . The usual RAE 2822 airfoil with 13 design variables is used, and the following thickness constraints are included:  $t/c \geq 0.0253$  at  $x/c = 0.01$ ,  $t/c \geq 0.121$  at  $x/c = 0.35$ ,  $t/c \geq 0.0137$  at  $x/c = 0.924$ , and  $t/c \geq 0.001516$  at  $x/c = 0.99$ . The weightings used are:  $\omega_L=1.0$ ,  $\omega_D=0.1$ ,  $\omega_P=1.0$ , and the design point weightings are even,  $w_{Mi}=1.0$ . As always, fully turbulent flow is assumed.

The Mach number/drag profile for Case 1 is plotted in Figure 5.1, as well as the pressure distributions for two design points:  $M=0.76$  with  $C_L=0.733$  and  $0.77$ . The drag profile is also compared to the initial design, the RAE 2822, at the respective conditions. At  $C_L=0.77$  the

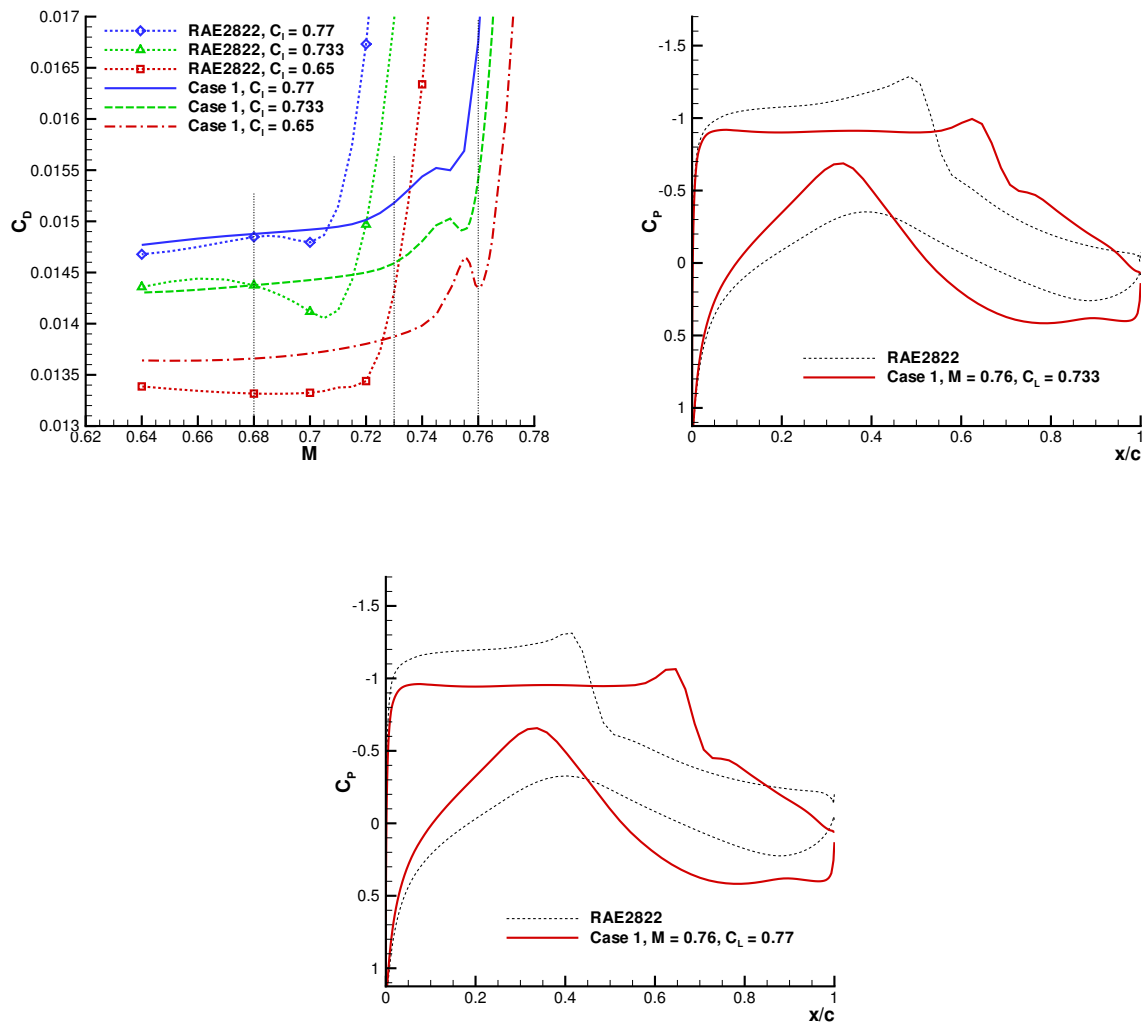


Figure 5.1: Nine-point Case 1.

$C_D$  curve shows a large drag reduction at the higher Mach number conditions ( $M=0.73$  and  $0.76$ ) with very little traded off at  $M=0.68$ . The same significant improvement for the other two lift conditions,  $C_L=0.733$  and  $0.65$ , is apparent at  $M=0.76$ . However, for  $C_L=0.65$  there is a larger increase in  $C_D$  at the lowest design point Mach number. The pressure distributions for  $M=0.76$  show that the shock has been weakened. Comparing the Mach number contours for the surrounding flow field, the large shocks displayed with the RAE 2822 in Figure 5.2 are significantly reduced for the Case 1 contours in Figure 5.3. The shock-induced separation also disappears.

Case 2 is identical to Case 1 except for using the 23-design variable parametrization mentioned earlier, from a 25 control-point B-spline. The resulting Mach number/drag sweeps are shown in

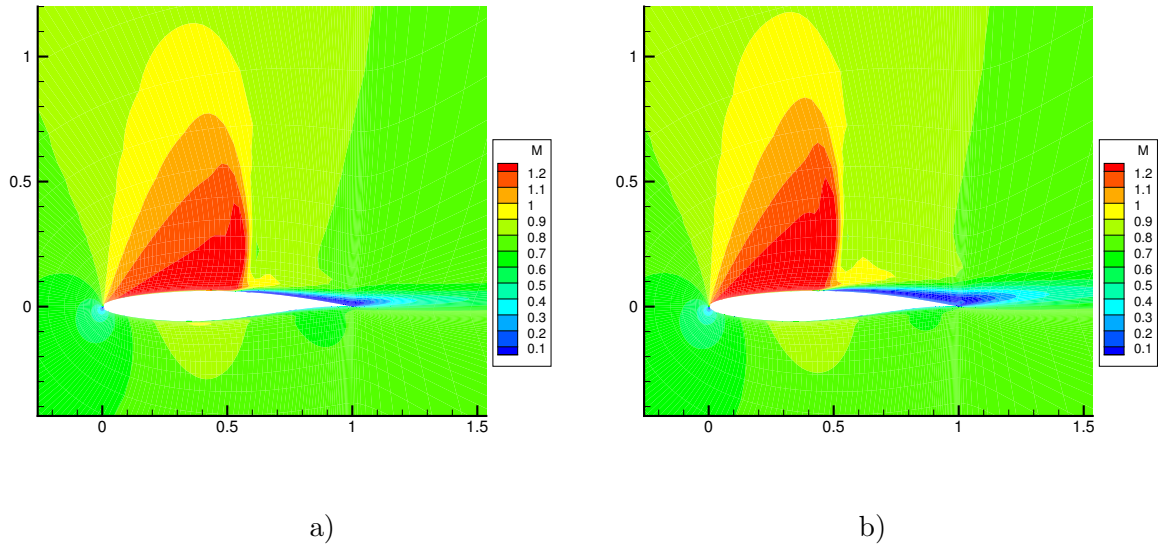


Figure 5.2: RAE 2822 Mach number contour graph at a)  $M=0.76$ ,  $C_L=0.733$ , b)  $M=0.76$ ,  $C_L=0.77$ .

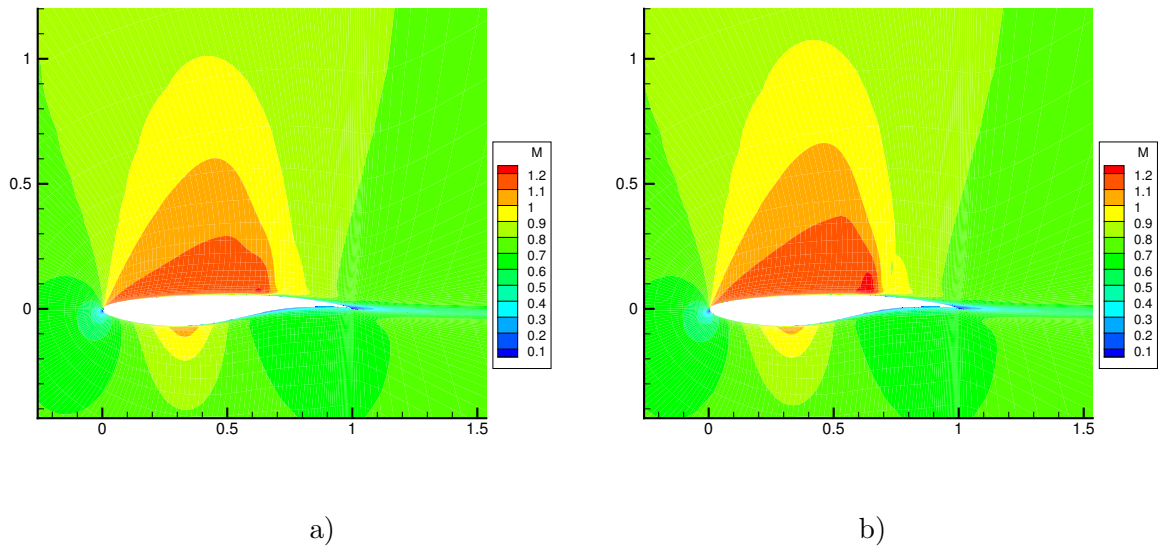


Figure 5.3: Nine-point Case 1 Mach number contour graph at a)  $M=0.76$ ,  $C_L=0.733$ , b)  $M=0.76$ ,  $C_L=0.77$ .

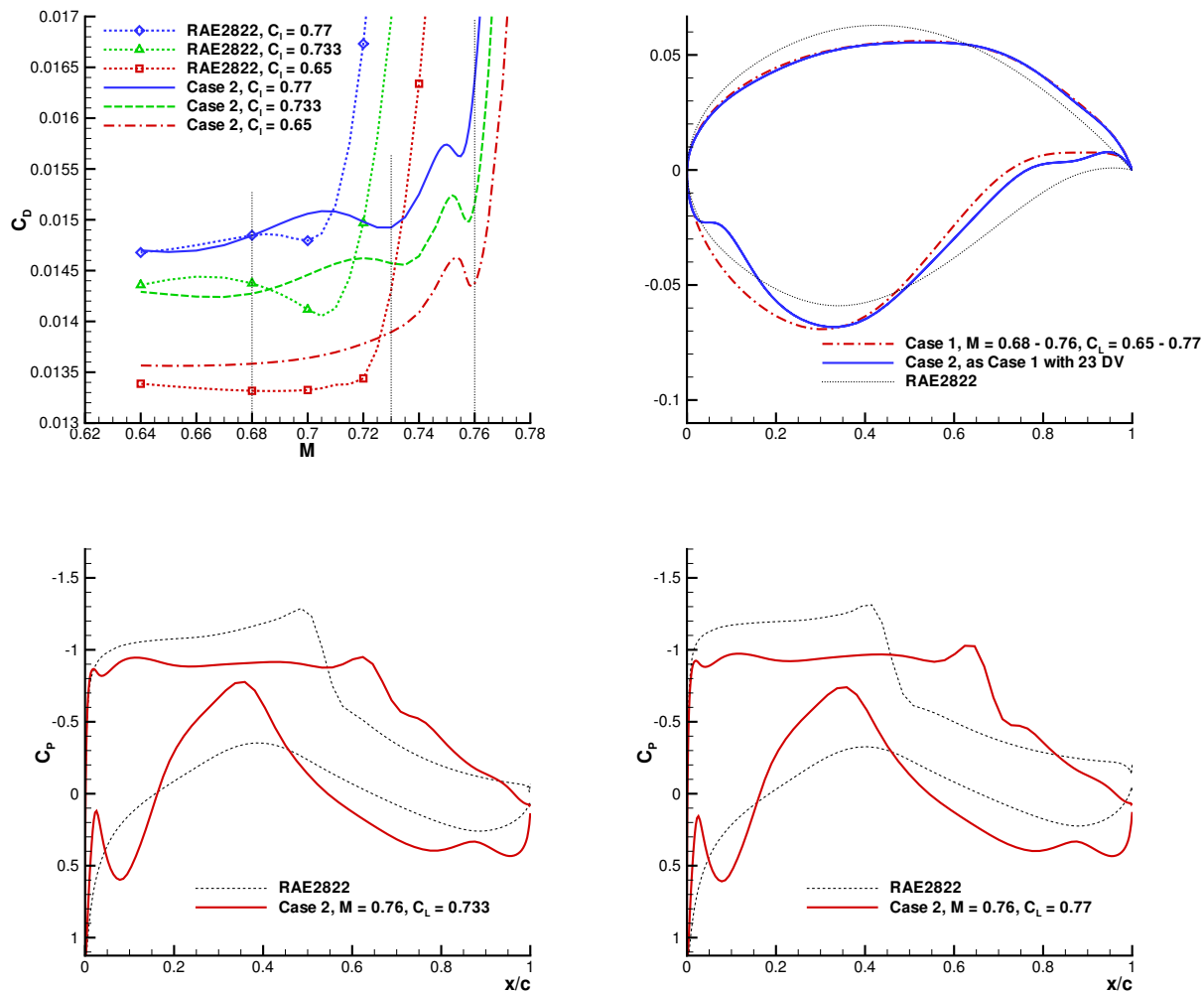


Figure 5.4: Nine-point Case 2 (23 DV instead of 13 DV).

Figure 5.4, with the Mach number contours shown in Figure 5.5. Comparing Cases 1 and 2 in Figure 5.6 shows an approximately 2%  $C_D$  reduction at  $M=0.76, C_L=0.77$  and  $0.733$  resulting from using more design variables. At  $M=0.68$ , the improvement is less than 1%, and it is even smaller at other design points. These improvements come at a cost, however, as off-design performance is worsened, such as at  $M=0.7, C_L=0.77$ . The greater geometric flexibility allows a more uneven  $C_D$  profile for the airfoil. The pressure distributions and airfoil shape also display a notch near the lower surface leading edge (Figure 5.4).

Case 3 is a 9-point problem with conditions identical to Case 1 (13 design variables), but with lower lift coefficient targets:  $C_L^* = 0.65, 0.715, \text{ and } 0.75$ . The same freestream  $M$  values are used. Figure 5.7 shows the Mach number/drag sweeps for all three  $C_L^*$  values compared to the initial RAE 2822 airfoil. The highest  $C_D$  curve for the highest lift coefficient target  $C_L=0.75$

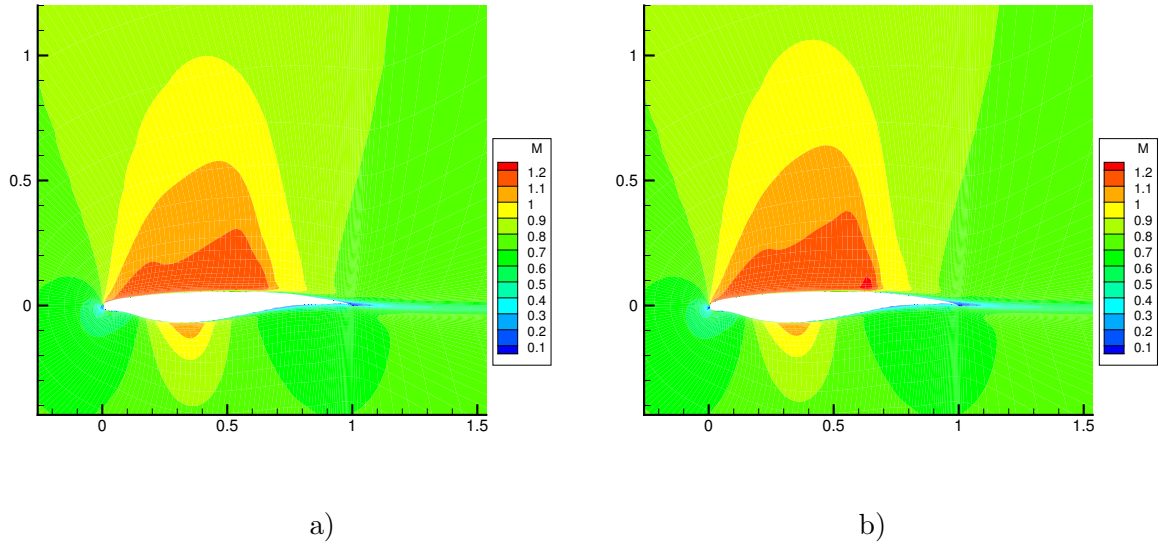


Figure 5.5: Nine-point Case 2 Mach number contour graph at a)  $M=0.76$ ,  $C_L=0.733$ , b)  $M=0.76$ ,  $C_L=0.77$ .

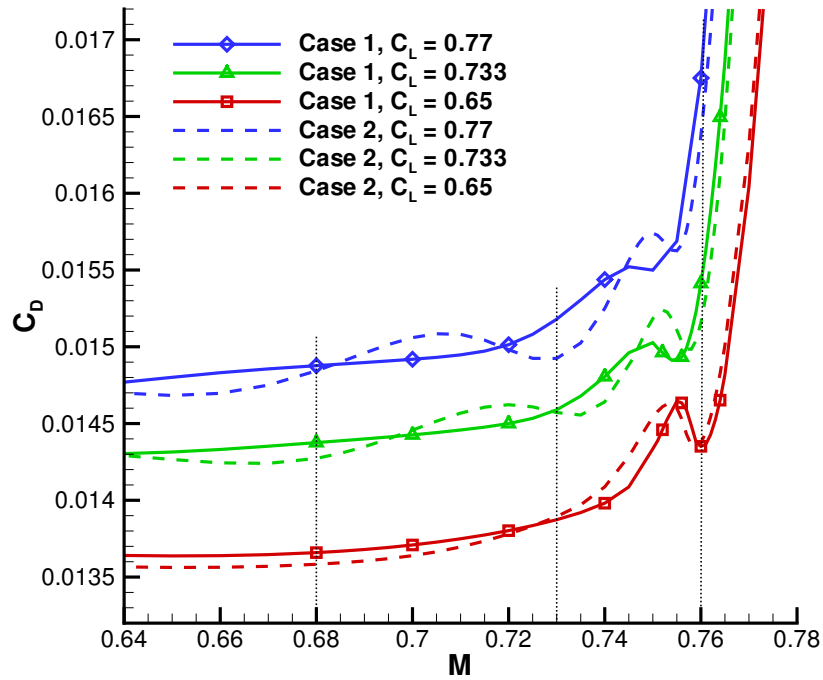


Figure 5.6: Comparison of Mach number/drag sweeps for the nine-point Cases 1 and 2 (13 DV vs. 23 DV).

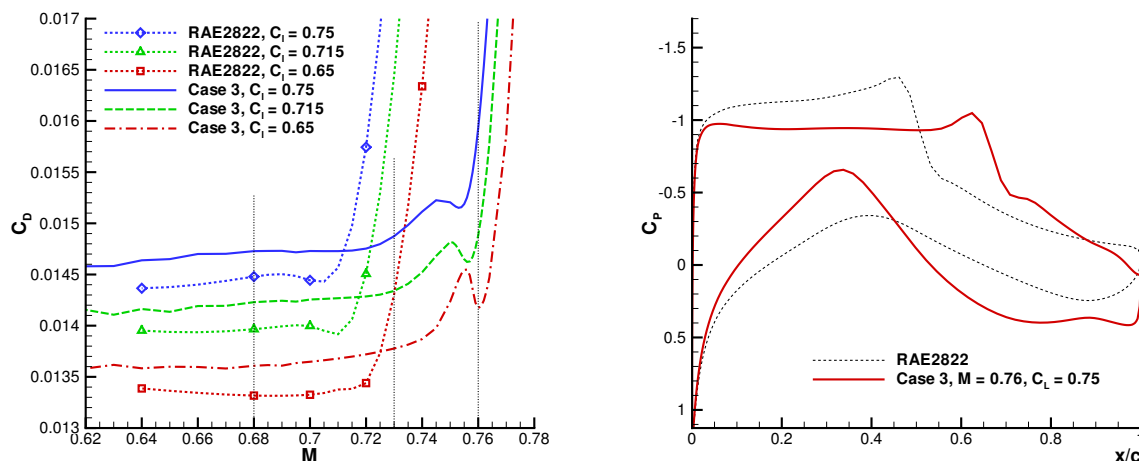


Figure 5.7: Nine-point Case 3.

does not show as clearcut an improvement as the  $C_L=0.77$  curve in Case 1 (Figure 5.1); while there is again a large drag reduction at  $M=0.76$ , there is a larger trade-off in performance around  $M=0.68$ . However for the three design points at  $C_L=0.65$ , which are shared with Case 1, Case 3 does manage a small drag reduction: 1.2% at  $M=0.76$ , 0.7% at  $M=0.73$ , and 0.4% at  $M=0.68$ . This is likely because the other 6 design points have a closer  $C_L$  target to the  $C_L=0.65$  design points than in Case 1, leading to a slightly easier optimization problem. It may also be because the highest  $C_L$  condition,  $C_L^*=0.75$ , did not show as broad an improvement over the Mach number range as the  $C_L^*=0.77$  points did in Case 1. Figure 5.8 shows the shock wave reduction in Mach contours for the initial and final airfoils in Case 3.

Case 4 has a more compact set of design point conditions than the previous 9-point cases, with Mach number range  $M=0.68, 0.705$ , and  $0.73$  and  $C_L^*=0.71, 0.725$ , and  $0.74$ . Since the highest  $M$  and  $C_L^*$  are lower than the previous cases, and the design point conditions are closer to each other in general, this optimization problem is clearly easier than the previous cases. All three  $C_D$  vs.  $M$  curves fall lower than the original RAE 2822 design at the same conditions, as shown in Figure 5.9. The improvement in the Mach number contour field is shown in Figure 5.10. While there were nine design points competing for drag minimization, the fact that the conditions were similar offered a predictable result, a broad improvement at all points. The airfoils for Cases 3 and 4 are shown in Figure 5.11.

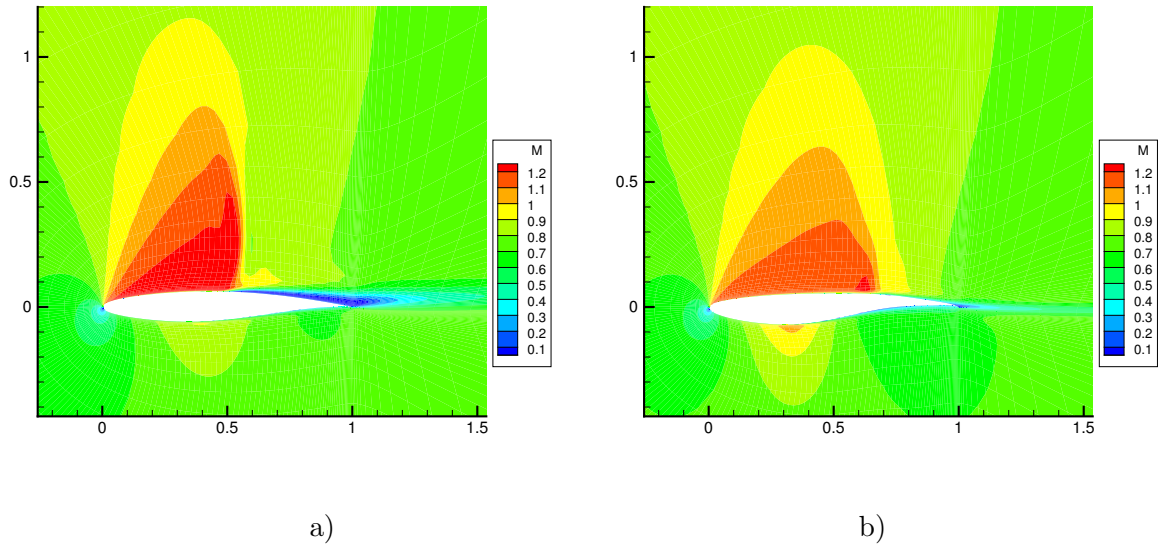


Figure 5.8: Mach number contour graph at  $M=0.76$ ,  $C_L=0.75$ , for a) RAE 2822, b) Case 3.

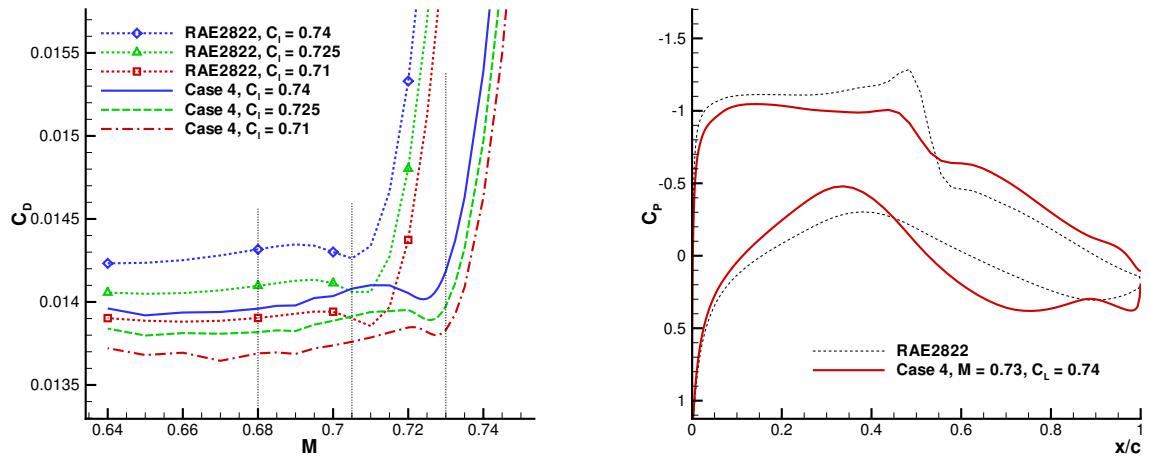


Figure 5.9: Nine-point Case 4.

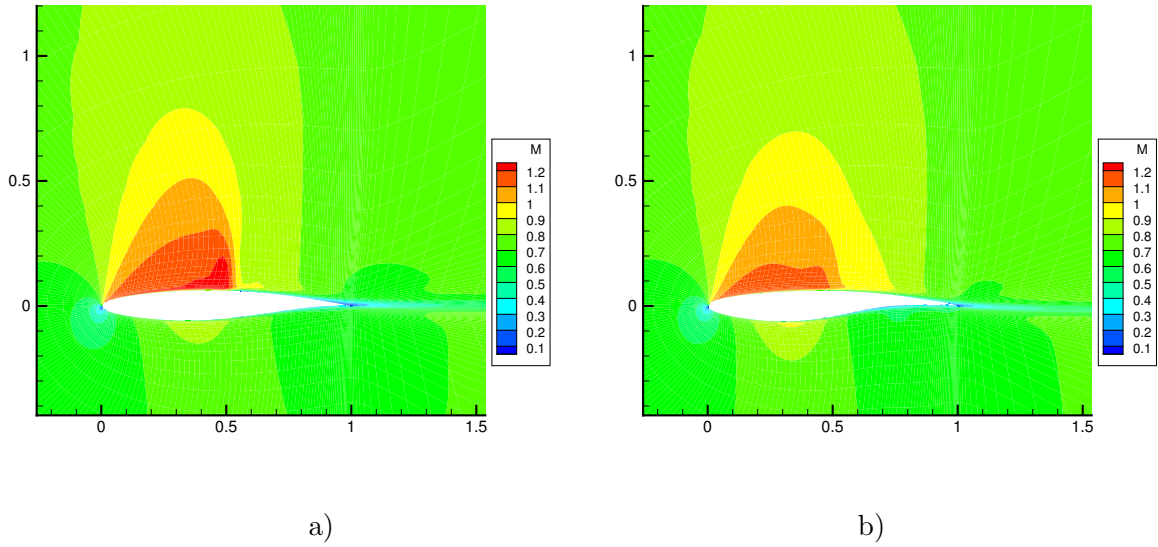


Figure 5.10: Mach number contour graph at  $M=0.73$ ,  $C_L=0.74$ , for a) RAE 2822, b) Case 4.

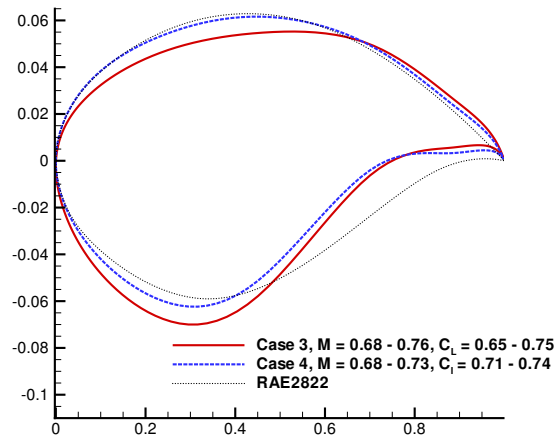


Figure 5.11: Final airfoils for nine-point cases 3 and 4.

## 5.2 Nine-point Automated Weights Cases

The multiple Mach number and lift coefficient target problem can be addressed with the automated weighting scheme discussed in the previous chapter, again with the goal being equalizing  $C_D$  between the different  $M$  values. However, since it is unrealistic to equalize the drag coefficients (across several Mach numbers) between design points with different  $C_L$  targets, Eq. 4.1 is applied to each set of  $M$  points with the same  $C_L^*$  as if it were a three point multi-point problem. Dividing the resulting weights by three conveniently makes them sum to one for a 9-point problem. The new weights are then used in the next iteration, as outlined before.

Case 5 uses this method on Case 1 in the previous section, with  $c = 15$ . The resulting weights and  $C_D$  values can be found in Tables 5.1 and 5.2. Table 5.3 shows useful values such as the sum of the standard deviation of each set of three design points at the same  $C_L^*$ , the sum of the maximum  $C_D$  from each set, and the standard deviation of all nine points taken together. The case is run for 6 iterations, at which point the sum of the standard deviations starts to rise; the best iteration is the fifth. At this point, two of the design points have been dropped,  $C_L=0.77$ ,  $M=0.73$ , and  $C_L=0.65$ ,  $M=0.68$ . By the fifth iteration, the sum of the maximum  $C_D$  for each set of lift coefficient targets is decreased by 2.8%, and the minimum  $C_D$  sum increased by 1.8% (after the first iteration, not from the initial RAE 2822 airfoil). The sum of standard deviations goes down to 0.000806. The  $C_D$  values at  $M=0.76$  go down an average of 3.6% after the first iteration, however those at  $M=0.73$  and 0.68 increase an average of 2.1%. Airfoil shapes and Mach number/drag sweeps are shown in Figure 5.12.

A problem with the method used in the previous case is that the sum of the weights for each set of design points with the same  $C_L^*$  is kept fixed. The optimization runs might generate a better airfoil if the weights were allowed to bias over time towards the more difficult, higher  $C_L$  target design points. To do this, a modified form of Eq. 4.1 is used:

$$w_i^{new} = \frac{\sum_{i=1}^{N_{C_L^*}} C_{Di}|_{C_L^*}}{\sum_{i=1}^N C_{Di}} \left[ w_i^{old} \frac{N}{N_{C_L^*}} + c \left( \frac{C_{Di}|_{C_L^*}}{\sum_{i=1}^{N_{C_L^*}} C_{Di}|_{C_L^*}} - \frac{1}{N_{C_L^*}} \right) \right] \quad (5.1)$$

where  $N_{C_L^*}$  is the number of sampling points at a specific  $C_L^*$ , and  $C_{Di}|_{C_L^*}$  is the  $C_D$  at a specific  $C_L^*$ . Since the drag coefficients at the higher  $C_L^*$  design points will be higher, the weights biased towards this set by the first term, which is the ratio of  $C_D$  totals between one set of  $C_L^*$  points and all the points.

Table 5.1: Nine-point Case 5 weights.

	$C_L=0.65$			Weights $C_L=0.733$			$C_L=0.77$		
	$M = 0.68$	<b>0.73</b>	<b>0.76</b>	<b>0.68</b>	<b>0.73</b>	<b>0.76</b>	<b>0.68</b>	<b>0.73</b>	<b>0.76</b>
1	0.11111	0.11111	0.11111	0.11111	0.11111	0.11111	0.11111	0.11111	0.11111
2	0.07502	0.10062	0.15769	0.06415	0.08823	0.18095	0.03361	0.06597	0.23376
3	0.05107	0.09306	0.18920	0.09583	0.05832	0.17919	0.06911	0.02035	0.24388
4	0.02333	0.08433	0.22568	0.11365	0.03259	0.18710	0.08217	0.00000	0.25117
<b>5</b>	<b>0.000000</b>	<b>0.074579</b>	<b>0.258754</b>	<b>0.127993</b>	<b>0.008092</b>	<b>0.197248</b>	<b>0.085666</b>	<b>0.000000</b>	<b>0.247667</b>
6	0.000000	0.061769	0.271564	0.138475	0.000000	0.194858	0.092629	0.000000	0.240704

Table 5.2: Nine-point Case 5 drag coefficients.

	$C_L=0.65$			$C_D$ $C_L=0.733$			$C_L=0.77$		
	$M = 0.68$	<b>0.73</b>	<b>0.76</b>	<b>0.68</b>	<b>0.73</b>	<b>0.76</b>	<b>0.68</b>	<b>0.73</b>	<b>0.76</b>
1	0.013659	0.013874	0.014352	0.014376	0.014589	0.015412	0.014877	0.015180	0.016750
2	0.013850	0.013988	0.014318	0.015198	0.014647	0.014899	0.015998	0.015236	0.015760
3	0.013800	0.013960	0.014341	0.015028	0.014640	0.014940	0.015790	0.015225	0.015839
4	0.013791	0.013954	0.014337	0.014989	0.014643	0.014951	0.015742	0.015228	0.015863
<b>5</b>	<b>0.013803</b>	<b>0.013963</b>	<b>0.014321</b>	<b>0.015032</b>	<b>0.014648</b>	<b>0.014943</b>	<b>0.015796</b>	<b>0.015230</b>	<b>0.015839</b>
6	0.013770	0.013935	0.014316	0.014909	0.014634	0.014984	0.015641	0.015226	0.015944

Table 5.3: Nine-point Case 5 performance characteristics.

	$\Sigma$ St. Dev.	St. Dev.	$\Sigma$ Range	$\Sigma$ Min $C_D$	$\Sigma$ Max $C_D$
1	0.001908	0.000930	0.003603	0.042912	0.046515
2	0.000906	0.000748	0.001781	0.043733	0.045514
3	0.000822	0.000728	0.001543	0.043665	0.045208
4	0.000807	0.000727	0.001527	0.043661	0.045189
<b>5</b>	<b>0.000806</b>	<b>0.000730</b>	<b>0.001512</b>	<b>0.043681</b>	<b>0.045192</b>
6	0.000825	0.000734	0.001615	0.043629	0.045244

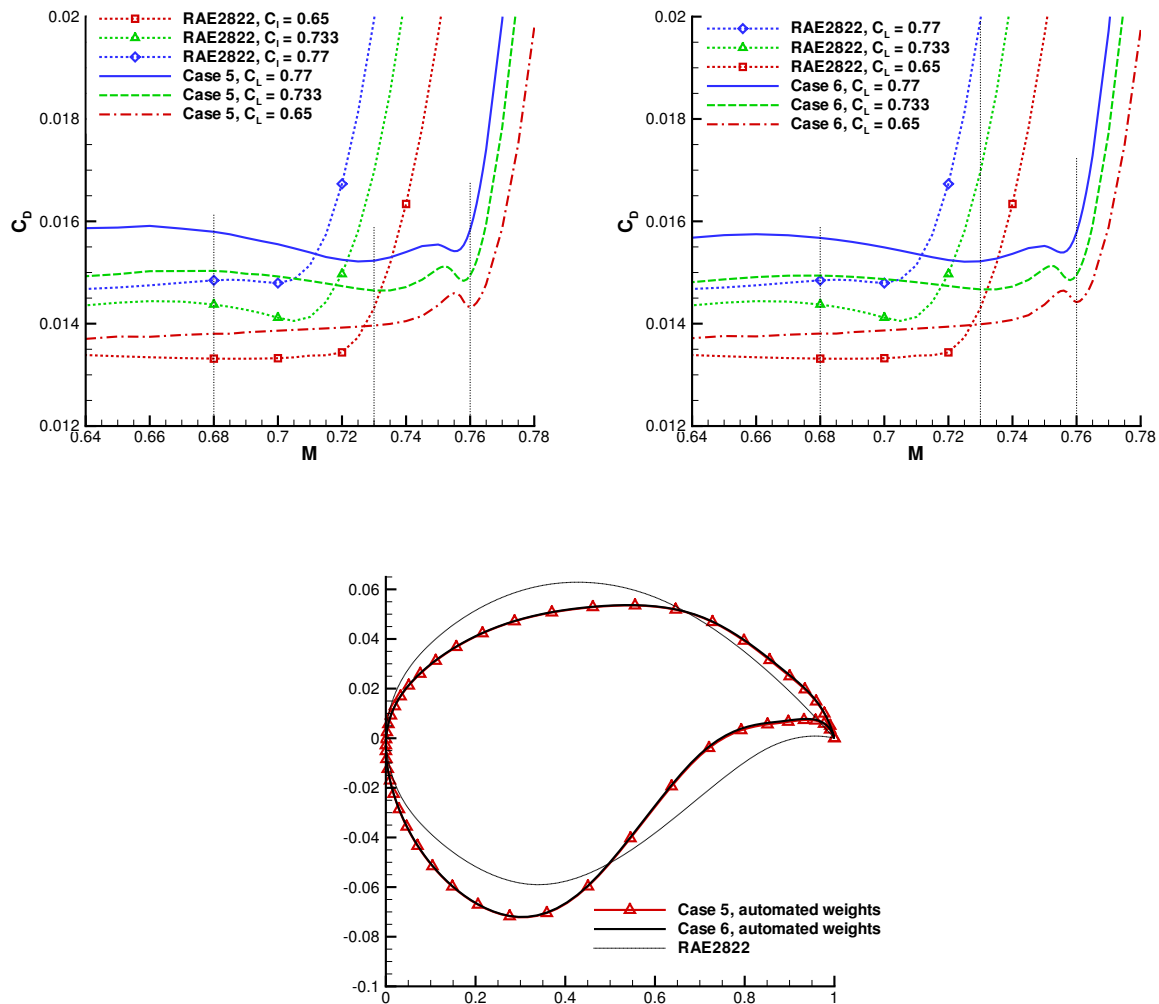


Figure 5.12: Mach number/drag sweeps and airfoils for nine-point Cases 5 and 6.

This new formula is used in Case 6, with the results listed in Tables 5.4-5.6. Mach number contour graphs for two design points are shown in Figure 5.13. The case is run through 8 weighting iterations, reducing the sum of the standard deviations to 0.000775, 0.000031 lower than Case 5. The sum of the maximum  $C_D$  values is 0.2% lower than Case 5, while the sum of the minimums is 0.15% higher. The average drag coefficient at  $M=0.76$  is reduced by 3.5% after the first iteration, slightly less than Case 5, while the rest are increased by an average of 1.9%, slightly more than Case 5. Overall, the design points at  $C_L=0.77$  are better improved, while  $C_D$  is increased for all three  $C_L=0.65$  points after the first iteration. This makes sense given that the weightings became biased towards the higher lift coefficient target. The final totals for the weights were 0.48 for  $C_L=0.77$ , 0.28 for  $C_L=0.733$ , and 0.24 for  $C_L=0.65$ . Several

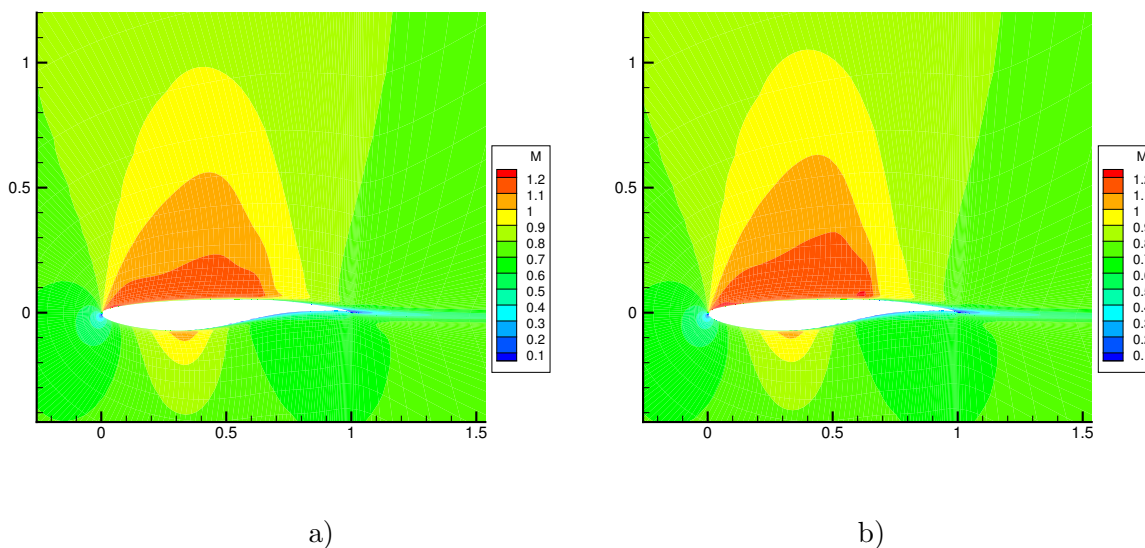


Figure 5.13: Nine-point Case 6 Mach number contour graph at a)  $M=0.76$ ,  $C_L=0.733$ , b)  $M=0.76$ ,  $C_L=0.77$ .

design points were also dropped midway, as shown in Table 5.4, effectively changing the original 9-point problem into a 6-point problem. However, after the design points were dropped,  $C_D$  at those points barely changed. In this case, the automated weighting method may have pointed out redundant design points. Final pressure distributions for all nine design points are shown in Figure 5.14, and all show the familiar shift in loading towards the trailing edge, with the mid-chord shocks at reduced at  $M=0.73$  and  $0.76$ .

The Mach number/drag sweeps and airfoils for Cases 5 and 6 are shown in Figure 5.12, along with a comparison to the RAE 2822 initial design (which shows that all three cases showed drastic drag reductions at higher Mach numbers). A comparison of the drag sweeps between Case 6 and Cases 1 and 2 (13 and 23 DV, which did not use the automatic weighting method) is shown in Figure 5.15. Except at  $C_L=0.65$ , Case 6 significantly outperforms both Cases 1 and 2 at  $M=0.76$ . Of course this is paid for by a trade-off in the lower Mach number range, at least partially an effect of the drag equalization goal of Case 6. A comparison of the airfoils for Cases 1, 2, and 6 is shown in Figure 5.16. The 13 design variable shapes are similar.

The 9-points cases show the behaviour of OPTIMA in a design cases with many design points, simultaneously across different Mach numbers and lift coefficient targets. In these cases, trade-offs have to be considered not only between performance at different Mach number conditions, but also between different lift requirements. A design case with design points that are spread too far across several difficult conditions will have higher greater problems and trade-offs than

Table 5.4: Nine-point Case 6 weights.

	$C_L=0.65$			Weights $C_L=0.733$			$C_L=0.77$		
	$M = 0.68$	<b>0.73</b>	<b>0.76</b>	<b>0.68</b>	<b>0.73</b>	<b>0.76</b>	<b>0.68</b>	<b>0.73</b>	<b>0.76</b>
1	0.11111	0.11111	0.11111	0.11111	0.11111	0.11111	0.11111	0.11111	0.11111
2	0.07084	0.09501	0.14890	0.06418	0.08827	0.18104	0.03547	0.06961	0.24667
3	0.04194	0.08204	0.17285	0.09552	0.05830	0.17982	0.07523	0.02522	0.26907
4	0.01235	0.06753	0.19550	0.11261	0.03273	0.18235	0.09984	0.00000	0.29709
5	0.000000	0.051411	0.209659	0.120073	0.009505	0.179138	0.115822	0.000000	0.314392
6	0.000000	0.036018	0.217304	0.123039	0.000000	0.172357	0.127256	0.000000	0.324027
7	0.000000	0.022371	0.223315	0.121332	0.000000	0.166870	0.133465	0.000000	0.332648
8	0.000000	0.010699	0.228357	0.119268	0.000000	0.162022	0.139002	0.000000	0.340651

Table 5.5: Nine-point Case 6 drag coefficients.

	$C_L=0.65$			$C_D$ $C_L=0.733$			$C_L=0.77$		
	$M = 0.68$	<b>0.73</b>	<b>0.76</b>	<b>0.68</b>	<b>0.73</b>	<b>0.76</b>	<b>0.68</b>	<b>0.73</b>	<b>0.76</b>
1	0.013659	0.013874	0.014352	0.014376	0.014589	0.015412	0.014877	0.015180	0.016750
2	0.013819	0.013974	0.014331	0.015176	0.014628	0.014884	0.015980	0.015213	0.015730
3	0.013811	0.013974	0.014372	0.015048	0.014654	0.014929	0.015814	0.015229	0.015791
4	0.013806	0.013977	0.014396	0.015002	0.014668	0.014940	0.015757	0.015234	0.015792
5	0.013805	0.013977	0.014401	0.014990	0.014669	0.014942	0.015740	0.015232	0.015793
6	0.013802	0.013982	0.014418	0.014952	0.014677	0.014958	0.015690	0.015230	0.015799
7	0.013804	0.013986	0.014419	0.014938	0.014668	0.014951	0.015675	0.015219	0.015789
8	0.013807	0.013989	0.014421	0.014940	0.014670	0.014952	0.015676	0.015218	0.015784

Table 5.6: Nine-point Case 6 performance characteristics.

	$\Sigma$ St. Dev.	St. Dev.	$\Sigma$ Range	$\Sigma$ Min $C_D$	$\Sigma$ Max $C_D$
1	0.001908	0.000930	0.003603	0.042912	0.046515
2	0.000928	0.000745	0.001827	0.043660	0.045487
3	0.000822	0.000717	0.001540	0.043694	0.045234
4	0.000794	0.000705	0.001483	0.043708	0.045190
5	0.000790	0.000702	0.001478	0.043706	0.045184
6	0.000779	0.000693	0.001465	0.043710	0.045175
7	0.000777	0.000687	0.001468	0.043692	0.045159
8	0.000775	0.000685	0.001462	0.043695	0.045156

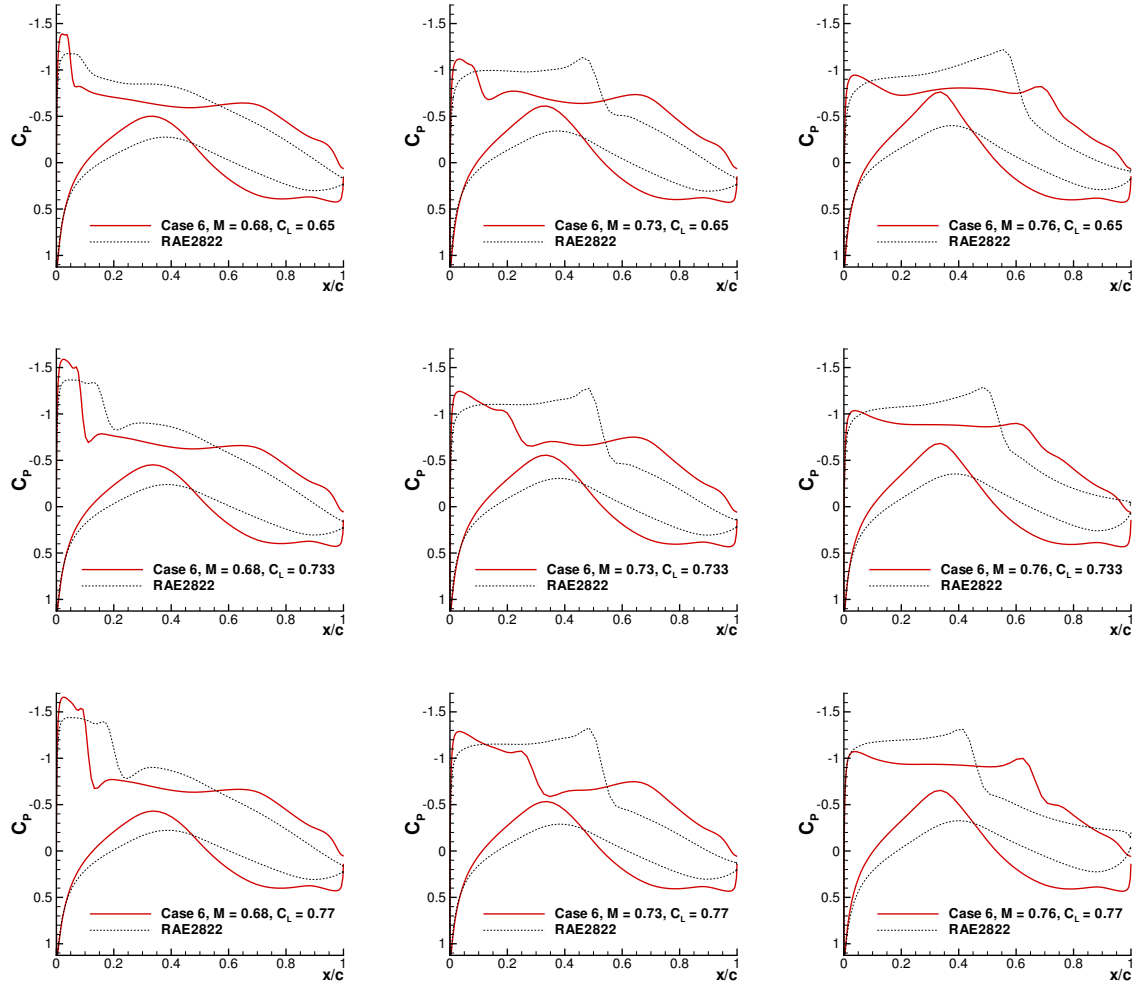


Figure 5.14: Case 6,  $C_p$  graphs for all nine design points.

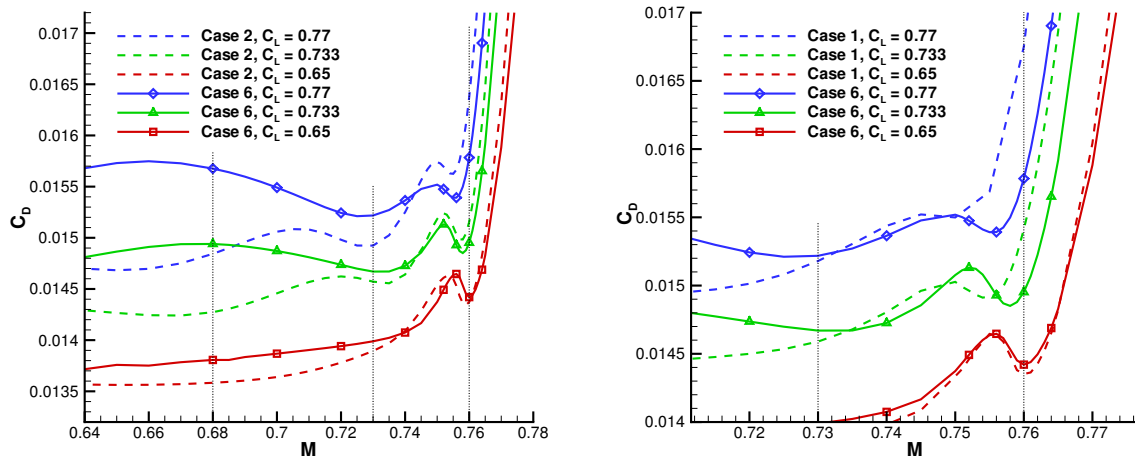


Figure 5.15: Comparison of Mach number/drag sweeps for the nine-point Cases 1, 2, and 6.

those that are more concentrated on a narrower set of conditions. The automated weighting formula can also be applied to such problems. Allowing the formula to show unequal bias between the different sets of points with the same  $C_L^*$  proved slightly more advantageous in this case. It also showed that certain design points can be dropped with apparently little disadvantage, simplifying the problem and identifying possibly redundant design points, which will improve as long as the rest of the design points do so.

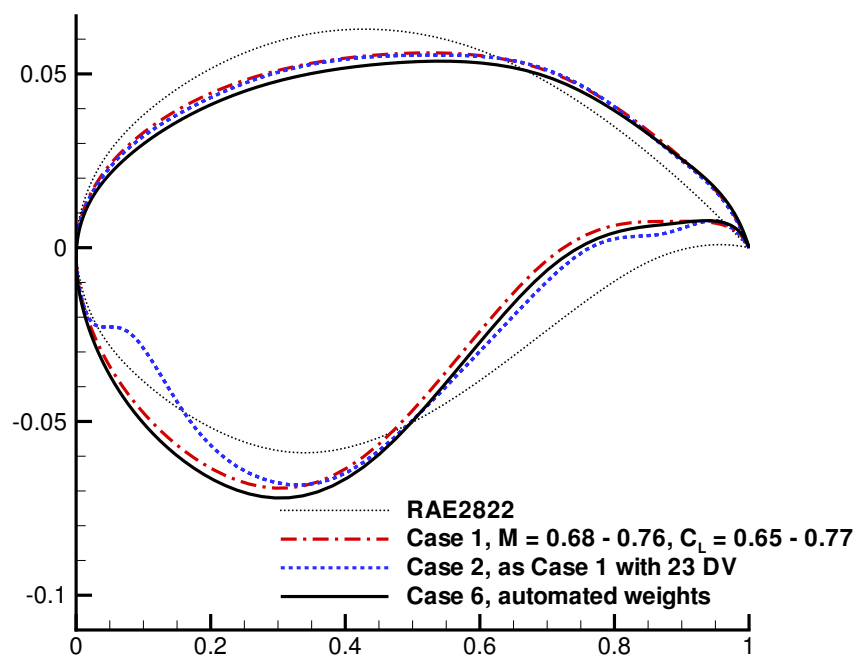


Figure 5.16: Comparison of airfoils for nine-point Cases 1, 2, and 6.

## Chapter 6

# Conclusions

A basic examination of the performance trade-offs, specifically the drag coefficient, in two-point optimization problems is conveniently summarized by the Pareto front plots (Figures 2.1 and 2.3). In these cases the unequal trade-off between the two design points combined with a designer's varying needs show that not all the points on the Pareto front are optimal cases in a practical sense. Certain points on the front are simply better than others, such as where the trade-offs become extremely favourable due to the steepness in the Pareto front. Different points on the front can also be considered desirable if further conditions are listed as being important to the designer (minimax  $C_D$ , integral of  $C_D$ ), and also indicate the preferable weightings to be used in such situations. While any coupling of weight values for the two-point design will produce a technically optimal solution (since it has been optimized), certain values prove advantageous in other respects.

The issue of weightings is further explored in the testing of an automated weighting formula (Eq. 4.1) for 4 and 5-point problems. The arbitrary goal of equalizing the drag coefficients in a multiple Mach number problem was met satisfactorily through the use of the formula, which reduced the standard deviation of the  $C_D$  values at the design points. The automated weighting formula is sensitive to the value of  $c$ , which, if set too high, can destabilize the problem over several iterations, or cause a repetitive cyclic trade-off that skips over the compromise solutions in between. Obviously a lower  $c$  can be chosen, or the method can be tempered by using the standard deviation variant method, although the two have very similar effects. The advantages of the latter may be in speeding up the process, although this is not the primary concern. If equal drag was desired across several Mach number values, the automated weight formula can successfully drive the solution towards that goal.

The automated weights formula can also reveal how certain design points can become redun-

dant. In one 9-point case (Table 5.4), several weights were reduced to zero, and yet the drag at those design points barely changed after they were taken out of the optimization problem. This can indicate that some design points, while perhaps important to a designer, do not necessarily need to be specified by the designer since improvements at other design points will have a desirable effect on these points anyways.

The 9-point cases also demonstrate the various possible trade-offs in a design problem with many design points, spread across several  $C_L$  and  $M$  values. The further the design points are from each other, the more complicated the trade-offs become, as several interacting factors compete with each other. This is one of the dangers, of course, of over-specifying a problem. More design points means a more difficult design problem, which may not satisfy a designer's requirements better than a problem which specifies all the requirements as part of the optimization problem (hence the advantage to simplifying the case by removing possible redundant design points). Problems with a large number of design points can reach a better solution by adding more design variables. However this can result in worse performance at off-design points, requiring the addition of more design points, which can in turn create a more difficult problem. It can also mean tolerating irregularities in the final airfoil shape, or having to specify more thickness constraints, which further limits the optimization process.

This leads to consideration of the appropriate method of geometrically constraining a problem. If the design requirements allow it, alternative constraint methods such as area constraints or a floating thickness constraint (not fixed to one chord location) can prove advantageous. They can give the optimization algorithm more freedom to find an optimal solution. The floating thickness constraint resulted in a maximum thickness location further towards the trailing edge than the initial RAE 2822 design. It also gave a virtually identical solution to the case that chose that same chord location with a fixed thickness constraint, meaning there is little drawback to using the floating thickness constraint in the cases shown. The area constraint proved advantageous in other ways, producing a slightly smoother-looking airfoil and keeping more of the mid-chord pressure loading than the rest of the cases. It tends to reduce the maximum thickness of the airfoil shape when compared to the thickness constraints; the thickness constraints, on the other hand, tend to have lower areas. If minimum thickness requirements are not an issue to the designer but area (or volume) is, the area constraint would be the more appropriate choice.

A variety of issues confront the designer formulating and running a multi-point optimization problem. The designer must understand the nature of the possible performance trade-offs when a problem is formulated, and needs to choose the right methods and techniques in order to apply appropriate weights, constraints, and design point choices to get the best solution from an optimization process. Improving the designer's understanding of these issues, and automating

as many inputs as possible, will help the designer get the most out of an optimization package.



# References

- [1] W. K. ANDERSON AND V. VENKATAKRISHNAN, *Aerodynamic design optimization on unstructured grids with a continuous adjoint formulation*, *Computers & Fluids*, 28 (1999), pp. 443–480.
- [2] O. BAYSAL AND K. GHAYOUR, *Continuous adjoint sensitivities for optimization with general cost functionals on unstructured meshes*, *AIAA Journal*, 39 (2001), pp. 48–55.
- [3] G. B. COSENTINO AND T. L. HOLST, *Numerical optimization design of advanced transonic wing configurations*, *Journal of Aircraft*, 23 (1986), pp. 192–199.
- [4] J. E. DENNIS JR. AND R. B. SCHNABEL, *Numerical Methods for Unconstrained Optimization and Nonlinear Equations*, Prentice-Hall Inc., Englewood Cliffs, N.J., 1983.
- [5] M. DRELA, *Pros & cons of airfoil optimization*, in *Frontiers of Computational Fluid Dynamics 1998*, D. A. Caughey and M. M. Hafez, eds., Singapore, 1998, World Scientific, pp. 363–381.
- [6] K. C. GIANNAKOGLU, *Design of optimal aerodynamic shapes using stochastic optimization methods and computational intelligence*, *Progress in Aerospace Sciences*, 38 (2002), pp. 43–76.
- [7] M. B. GILES AND M. DRELA, *Two-dimensional transonic aerodynamic design method*, *AIAA Journal*, 25 (1987), pp. 1199–1206.
- [8] P. E. GILL, W. MURRAY, AND M. A. SAUNDERS, *SNOPT: An SQP algorithm for large-scale constrained optimization*, *SIAM J. Optim.* Vol. 12, No. 4, pp. 979–1006, 2002.
- [9] P. E. GILL, W. MURRAY, AND M. H. WRIGHT, *Practical Optimization*, Academic Press Inc., Toronto, 1981.
- [10] D. E. GOLDBERG, *Genetic Algorithms in Search, Optimization, and Machine Learning*, Addison–Wesley, Reading, Mass., 1989.

- [11] T. L. HOLST AND T. H. PULLIAM, *Aerodynamic shape optimization using a real-number-encoded genetic algorithm*, AIAA Paper 2001-2473, Anaheim, CA, June 2001.
- [12] L. HUYSE AND R. M. LEWIS, *Aerodynamic shape optimization of two-dimensional airfoils under uncertain conditions*, NASA/CR-2001-210648, ICASE Report No. 2001-1, 2001.
- [13] A. JAMESON, *Aerodynamic design via control theory*, Journal of Scientific Computing, 3 (1988), pp. 233-260. Also ICASE report 88-64.
- [14] K. LEOVIRIYAKIT AND A. JAMESON, *Multi-point wing planform optimization via control theory*, Tech. Rep. Paper 2005-0450, American Institute of Aeronautics and Astronautics, 2005.
- [15] W. LI, L. HUYSE, AND S. PADULA, *Robust airfoil optimization to achieve drag reduction over a range of mach numbers*, Structural Multidisciplinary Optimization 24, 38-50, Springer-Verlag, 2002.
- [16] N. MARCO, J.-A. DÉSIDÉRI, AND S. LANTERI, *Multi-objective optimization in CFD by genetic algorithms*, Institut National De Recherche En Informatique Et En Automatique (INRIA), No. 3686, France, April 1999. Also see [www.lania.mx/~ccoello/EMOO/EMOObib.html](http://www.lania.mx/~ccoello/EMOO/EMOObib.html).
- [17] B. MOHAMMADI, *Practical applications to fluid flows of automatic differentiation for design problems*, in Inverse Design and Optimization Methods, 1997-05, von Kármán Institute For Fluid Dynamics, Brussels, Belgium, April 1997.
- [18] M. NEMEC, *Optimal Shape Design of Aerodynamic Configurations: A Newton-Krylov Approach*, PhD thesis, University of Toronto, Dept. of Aerospace Science and Engineering, 2003.
- [19] M. NEMEC AND D. W. ZINGG, *Towards efficient aerodynamic shape optimization based on the Navier-Stokes equations*, AIAA Paper 2001-2532, 2001.
- [20] ———, *From analysis to design of high-lift configurations using a Newton-Krylov algorithm*, Tech. Rep. Paper 173, ICAS 2002 Congress, 2002.
- [21] M. NEMEC AND D. W. ZINGG, *Newton-Krylov Algorithm for Aerodynamic Design Using the Navier-Stokes Equations*, AIAA Journal, 40 (2002), pp. 1146-1154.
- [22] M. NEMEC, D. W. ZINGG, AND T. H. PULLIAM, *Multi-point and multi-objective aerodynamic shape optimization*, AIAA paper 2002-5548, 2002.

- [23] E. J. NIELSEN AND W. K. ANDERSON, *Aerodynamic design optimization on unstructured meshes using the Navier Stokes equations*, AIAA Journal, 37 (1999), pp. 1411–1419.
- [24] J. NOCEDAL AND S. J. WRIGHT, *Numerical Optimization*, Springer–Verlag, New York, 1999.
- [25] S. OBAYASHI, *Aerodynamic optimization with evolutionary algorithms*, in Inverse Design and Optimization Methods, Lecture Series 1997-05, R. A. Van den Braembussche and M. Manna, eds., Brussels, Belgium, 1997, von Karman Institute for Fluid Dynamics.
- [26] ———, *Inverse optimization method for aerodynamic shape design.*, Recent Development of Aerodynamic Design Methodologies - Inverse Design and Optimization, K. Fujii and G. S. Dulikravich, Eds. Notes on Numerical Fluid Mechanics, 68 (1999).
- [27] A. OYAMA, *Wing Design Using Evolutionary Algorithms*, PhD thesis, Tohoku University, 2000.
- [28] Y. SAAD AND M. H. SCHULTZ, *GMRES: A generalized minimal residual algorithm for solving nonsymmetric linear systems*, SIAM J. Sci. Stat. Comput. Vol. 7, No. 3, 1986.
- [29] C. SUNG AND J. H. KWON, *Accurate aerodynamic sensitivity analysis using adjoint equations*, AIAA Journal, 38 (2000), pp. 243–250.
- [30] D. TSE AND L. CHAN, *Transonic airfoil design optimization using soft computing methods*, Canadian Aeronautics and Space Journal, 46 (2000), pp. 65–73.
- [31] P. WEINERFELT, *Aerodynamic optimization using control theory and surface mesh points as control variables*, FAU-97.044, SAAB, Linköping.
- [32] E. WHITNEY, L. GONZALEZ, K. SRINIVAS, AND J. PERIAUX, *Multi-criteria aerodynamic shape design problems in CFD using a modern evolutionary algorithm on distributed computers*, Proceedings of the Second International Conference on Computational Fluid Dynamics, 2002.
- [33] G. A. WRENN, *An indirect method for numerical optimization using the Kreisselmeier-Steinhauser function*, NASA CR-4220, March 1989.
- [34] F. ZHANG, S. CHEN, AND M. KHALID, *Multi-point optimization of transonic wing by real-coded genetic algorithm*, Proceedings of CFD2003, Vancouver, BC, 2003.

